EFFICIENT RESPONSE SURFACE METHOD FOR FATIGUE LIFE PREDICTION

By

Xinyu Chen

Thesis

Submitted to the Faculty of the

Graduate School of Vanderbilt University

In partial fulfillment of the requirements

for the degree of

MASTER OF SCIENCE

in

Civil Engineering

August, 2008

Nashville, Tennessee

Approved

Professor Sankaran Mahadevan

Professor Prodyot K. Basu

To my parents and wife

ACKNOWLEDGEMENT

This work would not have been possible without the guidance and support of many people. I thank all of my Thesis Committee members for their advice and suggestions. Especially to my thesis supervisor and mentor, Dr. Sankaran Mahadevan, I appreciate your guidance, inspiration, encouragement, and enthusiasm throughout my stay at Vanderbilt. As a successful scientist, erudite and diligent, you are an excellent model for me in both academics and personal life. I would like to thank Dr. Prodyot K. Basu for his advice, suggestions and direction on my graduate study.

I truly appreciate the friendship and technical support I received from Dr. Liming Liu throughout my graduate study. I am also thankful for the help and valuable discussions from our research group members, Chris Shantz, Venkata Sura, and Dr. Yongming Liu. Thanks to Dr. Xiaomo Jiang and all IGERT students for their encouragement and friendship.

I would like to extend my thanks to the Federal Aviation Administration and Department of Civil and Environmental Engineering at Vanderbilt for their financial support.

Finally I want to extend my most gracious and special thanks to my parents. Without the endless support and encouragement you have given me over the years, this could not have been completed.

TABLE OF CONTENTS

Page

LIST OF TABLES

Table Page

LIST OF FIGURES

Figure Page

CHAPTER I

INTRODUCTION

1.1 Overview

The growth properties of cracks that affect the reliability of mechanical structures are usually random. The randomness in crack growth properties result from variability in many factors such as external loading, geometry and material properties. For structures with complicated geometry, finite element analysis is needed for fatigue analysis. The combination of finite element method and structural reliability technique is necessary for probabilistic analysis of crack growth [1-3]. However, since the required many runs of finite element analysis can be expensive, a response surface can be used to approximate the finite element results and save the computational effort [4]. With this response surface, structural reliability can be easily evaluated with numerical methods such as Monte Carlo simulation.

Faravelli introduced stochastic finite element analysis coupled with the response surface method [5, 6] for the analysis of structural and mechanical systems whose geometrical and material properties have spatial random variability. This method used a polynomial expansion of the numerical nonlinear structural response, of which the actual analytical form is unknown. Newman and Raju built polynomial expansions of the stress intensity factors of cracks in three dimensional bodies based on finite element analysis [7, 8]. Many other research studies have used response surfaces based on polynomial expansion. However, although it is easy to implement, polynomial expansion may fail to

capture highly nonlinear structural response. Furthermore, the formulas of polynomial expansions such as the empirical equations proposed by Newman and Raju [7, 8] obtained from regression analysis may work for specific cases and may not be applicable to general cases. More accurate and efficient methods, thus, need to be developed.

A considerable amount of scatter is also found in fatigue data and happens even under the same loading condition. The reason for the phenomenon is due to the inhomogeneous material properties. To capture the statistical nature of fatigue crack growth data and save fatigue testing effort, many probabilistic models have been developed in recent years. Generally, these can be divided into two categories. The first one is to randomize the coefficients of an established deterministic model to represent material inhomogeneity [9]. The other is to generate the stochastic information by multiplying the deterministic dynamics of fatigue crack growth with a non-negative random process [10-13]. Fatigue crack growth is modeled by stochastic differential equations that require solutions of nonlinear partial differential equations [10-13]. These nonlinear partial differential equations known as the Kolmogorov's forward and backward equations can be solved numerically. Although these models are combined with crack growth laws and consider the physical mechanism, they are still based on data fitting to some extent. Furthermore, the computational effort is very intensive and the constraints in the models make them less accurate and robust.

This study proposes the application of a different type of response surface method – Gaussian process (GP) modeling – to fatigue crack growth analysis. Compared to the traditional response surface method such as polynomial expansion, this new method has been shown to be more accurate and efficient [12, 13], especially for highly nonlinear

relationships between multi-input and output variables. In this study, the computational effort of finite element analysis is shown to be significantly reduced in the fatigue crack analysis by using the GP model. The GP model can be also applied to fatigue growth data. The uncertainty in fatigue crack growth rate is captured by GP model. The powerful feature of GP model can reduce the fatigue test effort.

1.2 Research Objective and advantages of the proposed methodology

This study attempts to use an efficient method to capture the complicated relationship between input and output variables in fatigue crack growth analysis. Since traditional methods like polynomial expansions lack accuracy and are inefficient, a powerful statistical tool is needed. The application of GP modeling has the following advantages:

1. Accuracy: As mentioned above, the structural response may be highly nonlinear and multi-variate. GP modeling is able to capture the complex relationship between input and output variables and is particularly efficient in dealing with multi-variate problems (up to 30 or less).
2. Efficiency: To construct a response surface, several runs of finite element method are necessary, each run giving a training point for response surface fitting. For complicated structures, the finite element analysis to obtain each training point can be very time consuming. Further, the number of runs needed might be large. For example, if there are four input variables and one output variable, we shall take at least three values of input variables say maximum, minimum, and mean value to investigate the relationship between

inputs and output. Then 81 finite element runs are needed with one set, sometimes, taking a few hours. The reduction in finite element analysis may lead to the increasing error in the response surface. GP modeling can construct accurate response surfaces with significantly fewer training points than in traditional methods.

3. Versatility: In polynomial expansions, the forms and coefficients may work for a few specific cases and may not be applicable to all kinds of problems. Since GP modeling is non-parametric, no specific form is assumed, which make it more versatile and applicable to any kind of problem.

1.3 Organization of the thesis

The thesis is organized as follows: Chapter 2 introduces GP modeling. A basic idea of the method is first introduced. The procedure of parameter estimation is then described.

Chapter 3 compares GP modeling with polynomial-based response surfaces proposed by Newman and Raju [7, 8] for determining stress intensity factors of cracks in three dimensional finite bodies.

Chapter 4 extends the application of GP modeling to fatigue crack growth analysis in railroad wheels. In addition, other response surface models are compared with the GP model.

Chapter 5 applies the GP model to capture the statistics of fatigue data. Experimental data sets with two types of aluminum alloys are used for validation. An

adaptive sample selection procedure is implemented to improve the accuracy of the GP model.

CHAPTER II

GAUSSIAN PROCESS MODELING

2.1 Introduction

Gaussian process modeling is a statistical technique for interpolating data. Given its ability to fit any function form, the Gaussian process model is a good method to be used as a surrogate model to save expensive computational effort.

There are several features of Gaussian process model that make it attractive for use as the response surface model. First, it is a non-parametric model, which means that no specific form is assumed. Secondly, it is able to deal with multiple input variables and the number of input variables can go up to 30 [14]. Finally, the Gaussian process model can give not only the estimated values but also the uncertainty associated with these values of the unknown function at untested location. The estimated value is given as the mean value and the uncertainty is given as variance.

The basic idea of the Gaussian process model is that the values of the interpolated quantity at various coordinates are represented by a collection of random variables that have a joint normal distribution [14]. A Gaussian process is characterized by its mean function *m(x)* and covariance function *k(x)*. Thus, a Gaussian process, *Y*, can be denoted in terms of mean and covariance as

$$Y \sim N(m,k) \tag{1}$$

The mean function of the GP may capture systematic variations of the output *Y*. But the effect of the mean function for interpolating the training data is small. In this

study, we use a constant mean function. The covariance function is constructed as a function of the inputs, X. The basic idea of the covariance function is that when the inputs are close, the correlation between the corresponding outputs is high. So the mean function and covariance function can be expressed by:

$$E[Y(x)] = \beta \tag{2}$$

and

$$\text{cov}[Y(x), Y(x^*)] = \lambda^{-1} c(x, x^* | \phi) \tag{3}$$

where $c(x, x^* | \phi)$ is the correlation between x and x*, ϕ is the vector of parameters governing the correlation function, and λ is the process precision. So a Gaussian process is denoted by:

$$Y \sim N(\beta I, \lambda^{-1} R) \tag{4}$$

where R is the matrix of correlations among the training points. If the parameters in the mean and covariance function are known, the expected value and variance at any location x are calculated as

$$E[Y(x)] = \beta + r^T(x) R^{-1} (Y - \beta I) \tag{5}$$

and

$$Var[Y(x)] = \lambda^{-1} (1 - r^T R^{-1} r) \tag{6}$$

where r is the vector of correlations between x and each training point. Further, the covariance function at any location x are calculated as

$$\text{cov}[Y(x), Y(x^*)] = \lambda^{-1} (c(x, x^*) - r^T R^{-1} r_*) \tag{7}$$

where r_* is the vector of correlations between x^* and each training point.

There are a variety of possible parameterizations of the correlation function. The squared-exponential formulation has been commonly used as the correlation function [15], and is given by:

$$\mathrm{cov}[Y(x), Y(x^*)] = \exp[-\sum_{i=1}^{P} \phi_i (x_i - x_i^*)^2] \tag{8}$$

where p is the dimension of $\boldsymbol{x}$, and the parameters ϕ_i must be non-negative.

2.2 Parameter Estimation

The parameters λ, ϕ, and β in Eqs (5) through (8) need to be calibrated from the training points before applying Gaussian process modeling. Maximum likelihood estimation is the most common method to evaluate the values of the parameters.

As known, maximum likelihood estimation involves finding the likelihood function including parameters to evaluate. The likelihood function is based on the multivariate normal distribution at the training points. If the function is transformed into negative log of the likelihood function, the problem is to minimize the function by getting the optimal values of the parameters. The negative log of the likelihood function is given by:

$$-\log l(\phi, \beta, \lambda) = -m \log \lambda + \log|R| + \lambda (Y - \beta I)^T R^{-1} (Y - \beta I) \tag{9}$$

The numerical minimization of Eq. (8) can be expensive. The gradients are available in analytic form [14, 15]. The optimal values of the process mean and variance, conditional on the correlation parameters ϕ can be computed exactly. The optimal value of β is equivalent to the generalized least squares estimator:

$$\hat{\beta} = (I^T R^{-1} I)^{-1} I^T R^{-1} Y \tag{10}$$

However, Eq. (9) is highly susceptible to round off error, particularly when R is ill-conditioned. Better results have been obtained by using the ordinary least squares estimator, which in this case is simply the mean of Y. The conditional optimum for the process precision is given by

$$\hat{\lambda} = m[(Y - \beta I)^T R^{-1} (Y - \beta I)]^{-1} \tag{11}$$

2.3 Summary

This chapter introduced the basic ideas of the GP model and the procedure for parameter estimation in the model. In the next chapters, we will apply it to approximate the necessary quantities in crack growth modeling. Since it is too costly to get these quantities in both computational methods and fatigue tests, the idea is to model them as the output variables of the GP model to achieve savings in required efforts in computation and fatigue tests.

CHAPTER III

COMPARISON STUDY

3.1 Introduction

In linear fracture mechanics approach to crack growth modeling, the stress intensity factor (SIF) is a very significant quantity. The value of SIF is influenced by factors such as geometry, material properties, and loading. There is no explicit expression of SIF for some realistic problems and the calculation relies on finite element analysis. The change of crack size in each cycle leads to the change in SIF during each cycle of the fatigue life. However, it is computationally expensive to execute finite element analysis cycle by cycle. A response surface approximation is needed to approximately capture the relationship between the input variables and the output variable (SIF) using a few training points, by which the expensive computational effort in finite element analysis can be reduced. Then the calculation of SIF can be done by the surrogate model without using finite element analysis, and crack growth analysis can be done quickly.

Newman and Raju [7, 8] developed empirical stress intensity factor equations for 5 types of cracks subjected to remote uniaxial loading: embedded elliptical cracks, semielliptical surface cracks, quarter-elliptical corner cracks, semielliptical surface cracks at a hole, and quarter-elliptical corner cracks at a hole in finite plates. These equations consider SIF as a nonlinear function of loading, parametric angle, crack depth, crack length and plate thickness. For each case, the authors obtained the finite element results at many training points, using which empirical equations are built. Although the empirical

equations are within 5% of finite element results, it requires much effort to perform finite element analysis for all the training points and get accurate expressions for the response surface.

In this chapter, we compare GP modeling with the empirical equations developed by Newman and Raju [7, 8] and investigate the advantage of GP modeling. To avoid the error due to different implementations of finite element analysis, a part of the data obtained by Newman and Raju using finite element analysis [7, 8] is taken as the training points to construct GP modeling. The rest of the data is used for checking the accuracy of the prediction values. Then the results obtained from GP modeling are also compared with that from the empirical equations. Since Newman and Raju [7, 8] only gave the finite element results for the first four cases, the comparison between the two methods is done for the four cases.

3.2 Numerical examples

Figures 1 and 2 show the configuration of the 5 types of cracks in a three dimensional body.

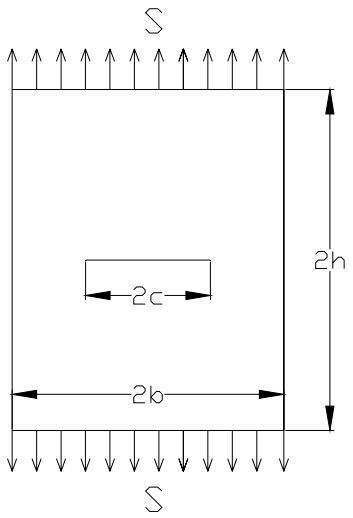

Figure 1 A finite plate with a center crack

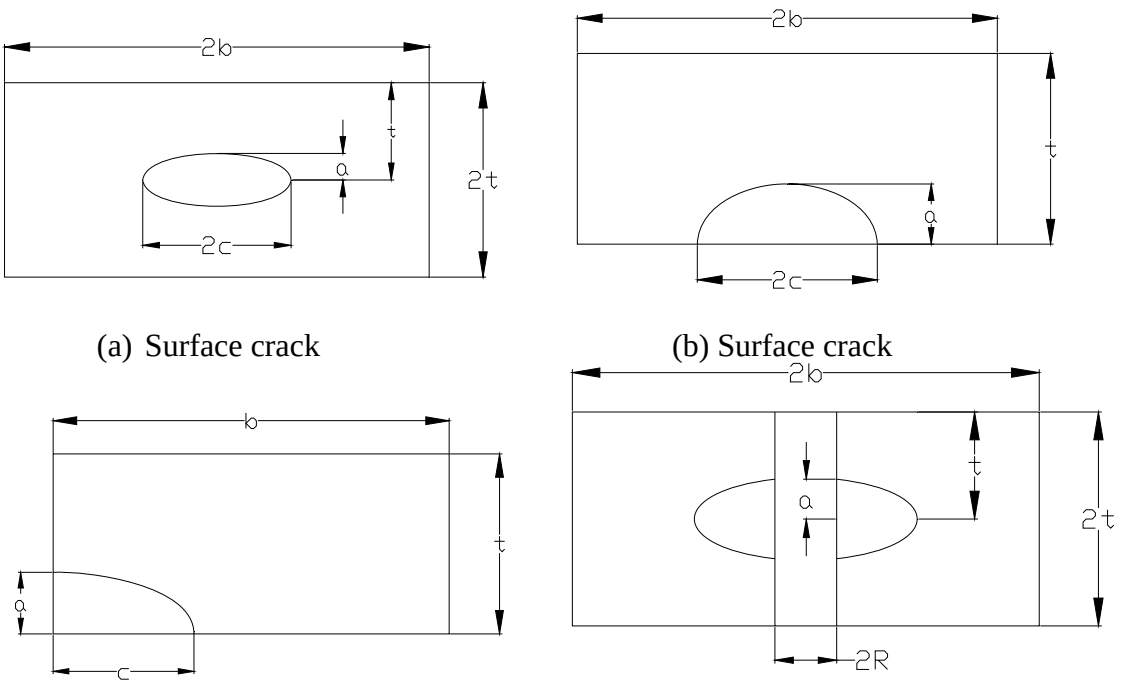

(a) Surface crack

(b) Surface crack

(c) Corner crack

(d) Surface crack at a hole

(d) Corner crack at a hole

Figure 2 Configuration of various cracks in three dimensional bodies

3.2.1 Empirical equations of stress intensity factor

The stress intensity factor, K_I, at the crack tip was expressed:

$$K_I = S\sqrt{\pi \frac{a}{Q}} F_S(\frac{a}{c}, \frac{a}{t}, \frac{c}{b}, \phi) \tag{12}$$

where Q is the shape factor for an ellipse. a is the crack depth, c is the crack length, t is the plate thickness and S is the external loading. The width b and the length h are large enough to be neglected. Parametric angle ϕ is the parameter to illustrate the different positions along the crack surface. F_S is the geometry factor. Figure 3 shows the coordinate system used to define it.

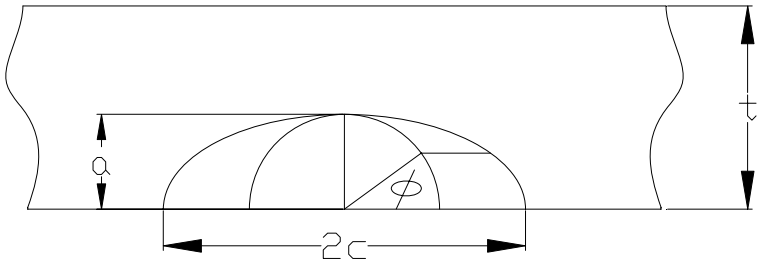

Figure 3 Coordinate system used to define the parametric angle

Empirical expressions for Q have been developed as

$$Q = 1 + 1.464(\frac{a}{c})^{1.65} \quad \text{for} \frac{a}{c} \le 1 \tag{13a}$$

$$Q = 1 + 1.464(\frac{c}{a})^{1.65} \quad \text{for} \frac{a}{c} > 1 \tag{13b}$$

Newman and Raju [7, 8] covered a wide range of configuration parameters. The ratio of crack depth to plate thickness (a/t) ranged from 0 to 1, the ratio of crack depth to crack length ranged from 0.2 to 2, the parametric angle ranged from 0 to $\frac{\pi}{2}$. Three-dimensional finite element analyses using singularity element were used to calculate the Mode I SIF for semi-elliptical surface cracks.

3.2.2 Semi-Elliptical surface crack

The geometry factors, F_S, obtained from the finite element results for the semi-elliptical surface crack in a finite plate subjected to tension are given in Table 1.

Table 1 *Geometry factors F_S for semi-elliptical surface cracks*

		a/t			
a/c	**2Φ/π**	**0.2**	**0.4**	**0.6**	**0.8**
	0	0.617	0.724	0.899	1.19
	0.125	0.65	0.775	0.953	1.217
	0.25	0.754	0.883	1.08	1.345
	0.375	0.882	1.009	1.237	1.504
0.2	0.5	0.99	1.122	1.384	1.657
	0.625	1.072	1.222	1.501	1.759
	0.75	1.128	1.297	1.581	1.824
	0.875	1.161	1.344	1.627	1.846
	1	1.173	1.359	1.642	1.851
	0	0.767	0.896	1.08	1.318
	0.125	0.781	0.902	1.075	1.285
	0.25	0.842	0.946	1.113	1.297
	0.375	0.923	1.01	1.179	1.327
0.4	0.5	0.998	1.075	1.247	1.374
	0.625	1.058	1.136	1.302	1.408
	0.75	1.103	1.184	1.341	1.437
	0.875	1.129	1.214	1.363	1.446
	1	1.138	1.225	1.37	1.447

	0	0.916	1.015	1.172	1.353
	0.125	0.919	1.004	1.149	1.304
	0.25	0.942	1.009	1.142	1.265
	0.375	0.982	1.033	1.16	1.24
0.6	0.5	1.024	1.062	1.182	1.243
	0.625	1.059	1.093	1.202	1.245
	0.75	1.087	1.121	1.218	1.26
	0.875	1.104	1.139	1.227	1.264
	1	1.11	1.145	1.23	1.264
	0	1.174	1.229	1.355	1.464
	0.125	1.145	1.206	1.321	1.41
	0.25	1.105	1.157	1.256	1.314
	0.375	1.082	1.126	1.214	1.234
1	0.5	1.067	1.104	1.181	1.193
	0.625	1.058	1.088	1.153	1.15
	0.75	1.053	1.075	1.129	1.134
	0.875	1.05	1.066	1.113	1.118
	1	1.049	1.062	1.107	1.112
	0	0.821	0.848	0.866	0.876
	0.125	0.794	0.818	0.833	0.839
	0.25	0.74	0.759	0.771	0.775
	0.375	0.692	0.708	0.716	0.717
2	0.5	0.646	0.659	0.664	0.661
	0.625	0.599	0.609	0.61	0.607
	0.75	0.552	0.56	0.56	0.554
	0.875	0.512	0.519	0.519	0.513

1	0.495	0.501	0.501	0.496

Based on Table 1, the empirical equations for geometry factors based on the finite element results were developed by Newman and Raju [7] as follows:

$$F_S = [M_1 + M_2(\frac{a}{t})^2 + M_3(\frac{a}{t})^4]gf_\phi f_w \tag{14}$$

$$f_w = [\sec(\frac{\pi c}{2b}\sqrt{\frac{a}{t}})]^{1/2} \tag{15}$$

For $a/c \geq 1$

$$M_1 = \sqrt{\frac{c}{a}}(1 + 0.04\frac{c}{a}) \tag{16}$$

$$M_2 = 0.2(\frac{c}{a})^4 \tag{17}$$

$$M_3 = -0.11(\frac{c}{a})^4 \tag{18}$$

$$g = 1 + [0.1 + 0.35(\frac{c}{a})(\frac{a}{t})^2](1 - \sin\phi)^2 \tag{19}$$

$$f_\phi = [(\frac{a}{c})^2 \cos^2\phi + \sin^2\phi]^{1/4} \tag{20}$$

For $a/c \geq 1$

$$M_1 = 1.13 - 0.09(\frac{a}{c}) \tag{21}$$

$$M_2 = -0.54 + \frac{0.89}{0.2 + (\frac{a}{c})} \tag{22}$$

$$M_3 = 0.5 - \frac{1}{0.65 + (\frac{a}{c})} + 14(1 - \frac{a}{c})^{24} \tag{23}$$

$$g = 1 + [0.1 + 0.35(\frac{a}{t})^2](1 - \sin\phi)^2 \tag{24}$$

$$f_\phi = [(\frac{c}{a})^2 \sin^2\phi + \cos^2\phi]^{1/4} \tag{25}$$

From the above, it is obvious that the empirical equations developed by Newman and Raju are complicated and require much computational effort. It is also very time-consuming to get all the 180 training points by finite element analysis.

First, 27 points (a/c is 0.2, 0.6, 2.0, a/t is 0.2, 0.4, 0.8, and ϕ is 0, 0.5, 1) are picked as the training points. The GP model constructed with these 27 points is used to predict the SIF values at the other 80 points (a/c is 0.2, 0.4, 0.6, 1.0, 2.0, a/t is 0.2, 0.4, 0.6, 0.8, and ϕ is 0.125, 0.375, 0.625, and 0.875). The prediction values from the Newman - Raju empirical equations are also shown for comparison. Figure 4 shows the results in Table 1 and the prediction values from GP modeling and the empirical equations.

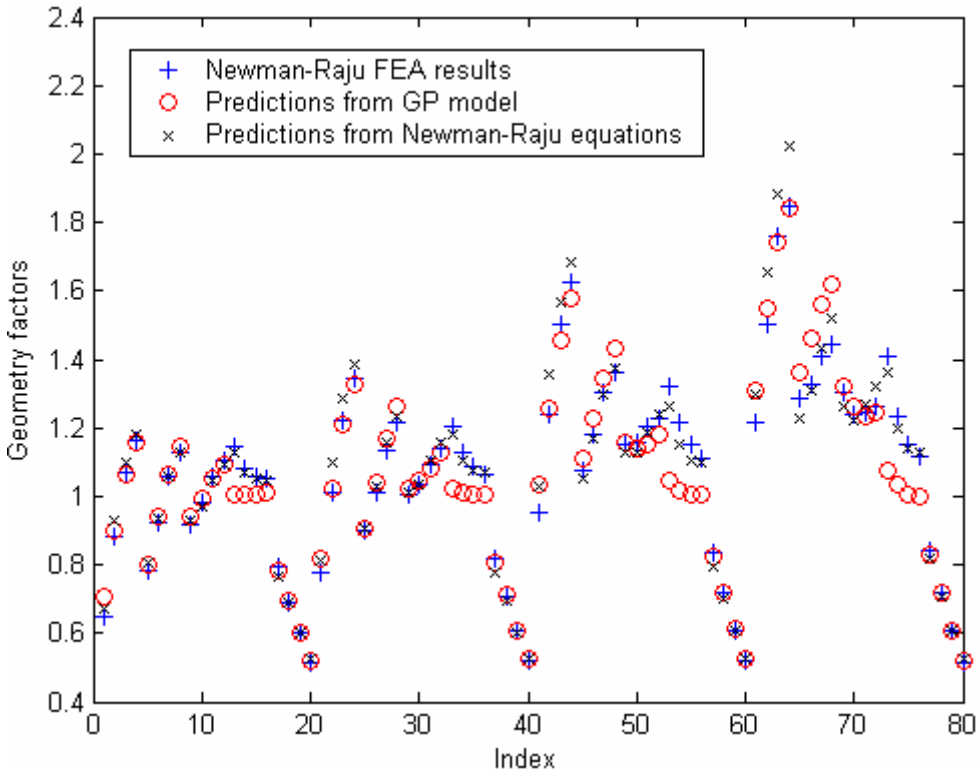

Figure 4 Comparison for semi-elliptical crack with 27 training points

The average error of GP modeling is:

$$Error = \frac{1}{80}\sum\left|\frac{F_{FEA} - F_{GP}}{F_{FEA}}\right| = 4.36\%$$

The maximum error is 23.85%. The minimum error is 0.02%. The errors at 13 points are greater than 10%, out of 80 validation points.

The average error of the empirical equations is:

$$Error = \frac{1}{80}\sum\left|\frac{F_{FEA} - F_{Eq}}{F_{FEA}}\right| = 2.61\%$$

Next, 36 points (a/c is 0.2, 0.6, 1.0, 2.0, a/t is 0.2, 0.4, 0.8, and ϕ is 0, 0.5, 1) are used as training points. The same 80 points are used for the prediction. Figure 5 shows the results in Table 1 and the prediction values from GP modeling.

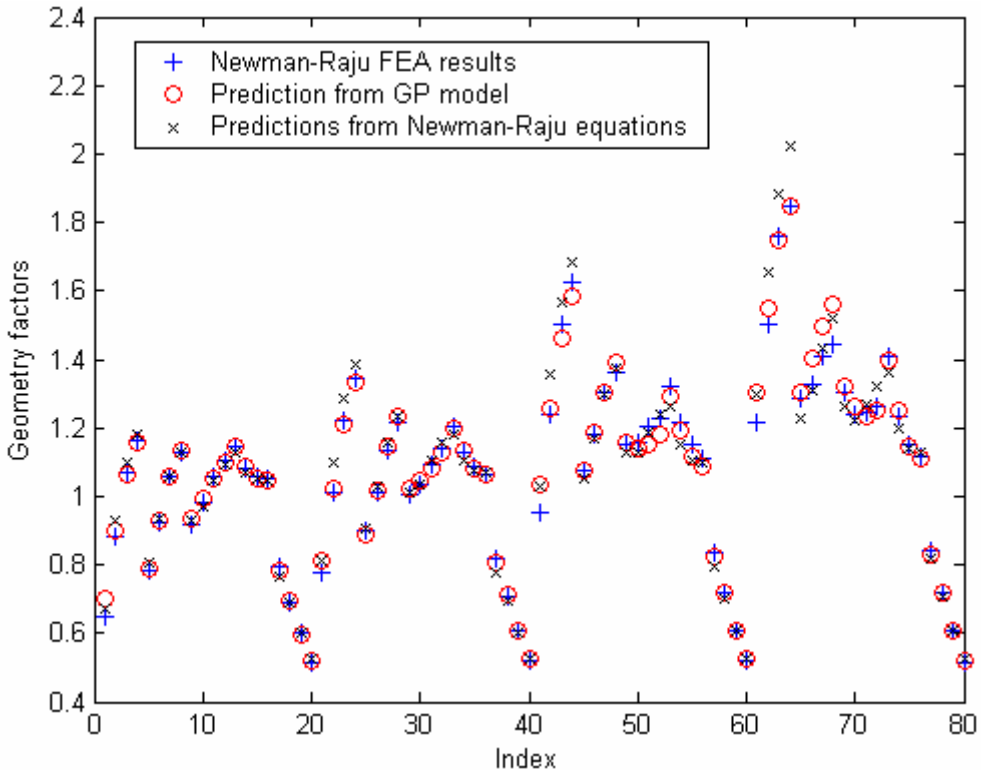

Figure 5 Comparison for semi-elliptical cracks with 36 training points

The average error of GP modeling is:

$$Error = \frac{1}{80}\sum\left|\frac{F_{FEA} - F_{GP}}{F_{FEA}}\right| = 1.64\%$$

The maximum error is 8.34%. The minimum error is 0.02%. The errors at all points are less than 10%, out of 80 validation points.

Finally, 60 points (a/c is 0.2, 0.4, 0.6, 1.0, 2.0, a/t is 0.2, 0.4, 0.6, 0.8, and ϕ is 0, 0.5, 1) are used as training points. Figure 6 shows the results in Table 1 and the prediction values from GP modeling.

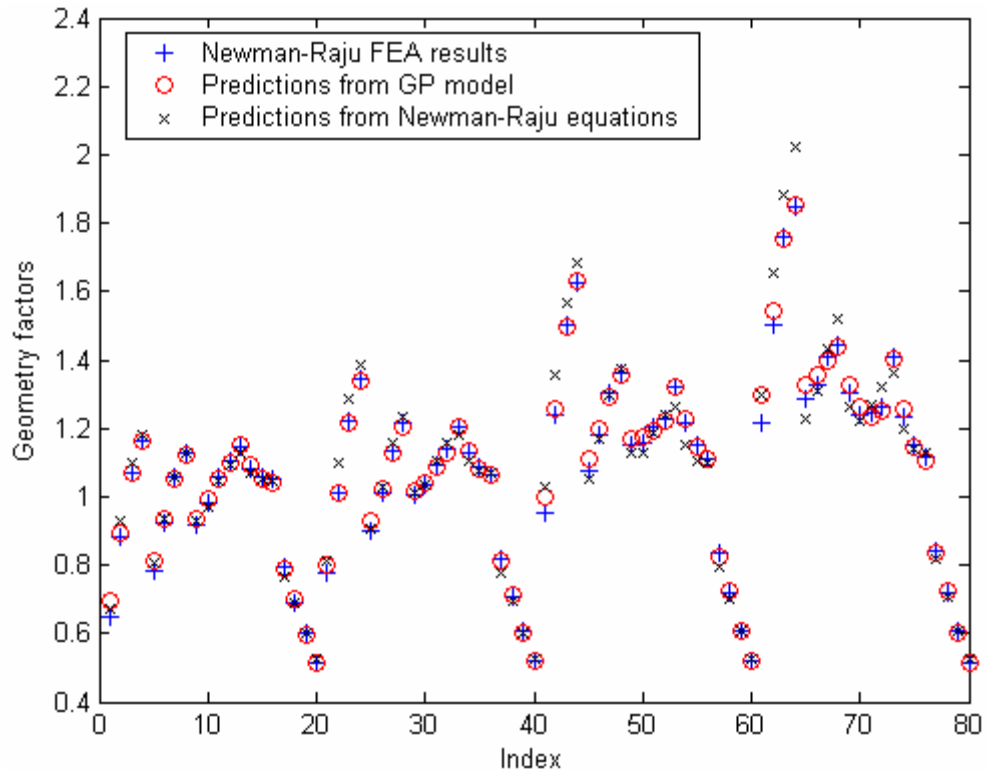

Figure 6 Comparison for semi-elliptical cracks with 60 training points

The average error of GP modeling is:

$$Error = \frac{1}{80}\sum\left|\frac{F_{FEA} - F_{GP}}{F_{FEA}}\right| = 1.17\%$$

The maximum error is 6.63%. The minimum error is 0%. The errors at all points are less than 10%, out of 80 validation points.

Figure 7 shows the average GP model error with the various numbers of training points. When the number of training points is 75, the average error is 0.4%. With the increasing number of training points, the error in the GP model decreases.

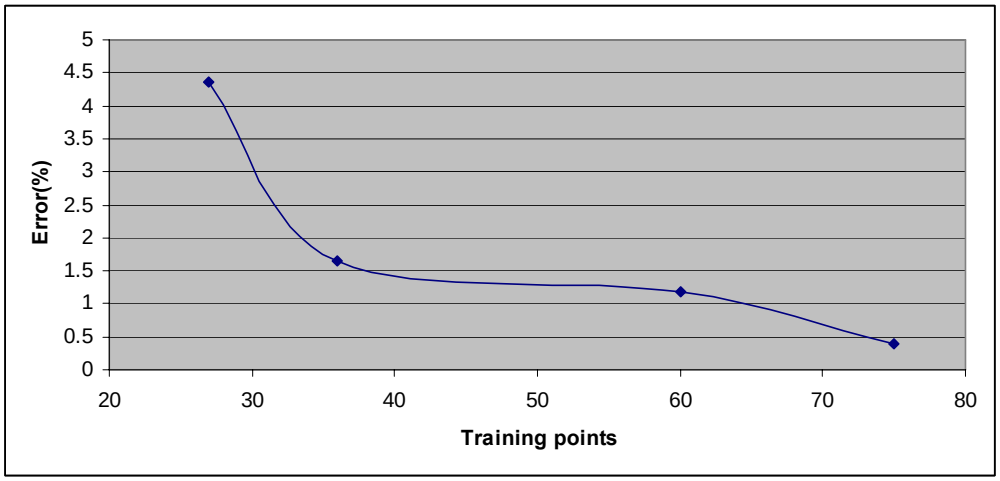

Figure 7 Average GP model error with various numbers of training points

3.2.3 Embedded Elliptical Crack

Values of the geometry factor, F_S, obtained from the finite element results for the embedded elliptical crack in a finite plate subjected to tension are given in Table 2.

Table 2 *Geometry factors F for embedded elliptical crack* ($c/b \le 0.2; h/b = 1; \nu = 0.3$)

		a/t		
a/c	**2Φ/π**	**0.2**	**0.5**	**0.8**
	0	0.45	0.473	0.514
	0.125	0.531	0.556	0.605
	0.25	0.643	0.678	0.745
	0.375	0.75	0.794	0.884
0.2	0.5	0.838	0.893	1.015
	0.625	0.905	0.978	1.176

	0.75	0.951	1.042	1.329
	0.875	0.978	1.083	1.438
	1	0.987	1.097	1.48
	0	0.632	0.66	0.721
	0.125	0.656	0.685	0.749
	0.25	0.715	0.748	0.821
	0.375	0.789	0.826	0.905
0.4	0.5	0.857	0.9	0.995
	0.625	0.914	0.964	1.105
	0.75	0.954	1.014	1.211
	0.875	0.978	1.046	1.285
	1	0.987	1.056	1.312
	0	0.986	1.009	1.06
	0.125	0.986	1.009	1.058
	0.25	0.986	1.008	1.05
	0.375	0.986	1.006	1.035
1	0.5	0.986	1.006	1.036
	0.625	0.986	1.008	1.059
	0.75	0.986	1.01	1.093
	0.875	0.986	1.012	1.114
	1	0.986	1.013	1.121
	0	0.709	0.713	0.72
	0.125	0.703	0.707	0.714
	0.25	0.686	0.69	0.697
	0.375	0.658	0.662	0.669

2	0.5	0.622	0.625	0.633
	0.625	0.579	0.582	0.592
	0.75	0.536	0.539	0.552
	0.875	0.503	0.506	0.522
	1	0.49	0.494	0.511

Based on Table 2, the empirical equations for embedded elliptical crack as follows:

$$F_S = [M_1 + M_2(\frac{a}{t})^2 + M_3(\frac{a}{t})^4]gf_\phi f_w \tag{26}$$

$$f_w = [\sec(\frac{\pi c}{2b}\sqrt{\frac{a}{t}})]^{1/2} \tag{27}$$

For $a/c \le 1$

$$M_1 = 1 \tag{28}$$

$$M_2 = \frac{0.05}{0.11 + (\frac{a}{c})^{3/2}} \tag{29}$$

$$M_3 = \frac{0.29}{0.23 + (\frac{a}{c})^{3/2}} \tag{30}$$

$$g = 1 - \frac{(\frac{a}{t})^4}{1 + 4(\frac{c}{a})}|\cos\phi| \tag{31}$$

$$f_\phi = [(\frac{a}{c})^2 \cos^2\phi + \sin^2\phi]^{1/4} \tag{32}$$

For $a/c > 1$

$$M_1 = \sqrt{\frac{c}{a}} \tag{33}$$

$$f_\phi = [(\frac{c}{a})^2 \sin^2\phi + \cos^2\phi]^{1/4} \tag{34}$$

The functions M_2, M_3, g and f_w are given by Eq 29, 30, 31, and 27, respectively.

As *a/c* approaches zero and ϕ equals $\pi/2$, the stress intensity factor equation reduces to

$$K_I = S\sqrt{\pi \frac{a}{Q}}[1 + 0.455(\frac{a}{t})^2 + 1.261(\frac{a}{t})^4] \tag{35}$$

As *a/c* approaches zero infinity and ϕ equals zero, the equations reduce to

$$K_I = S\sqrt{\pi \frac{a}{Q}}[\sec(\frac{\pi c}{2b}\sqrt{\frac{a}{t}})]^{1/2} \tag{36}$$

First, 27 points (a/c is 0.2, 0.4, 2.0, a/t is 0.2, 0.5, 0.8, and ϕ is 0, 0.5, 1) in Table 1 are picked as the training points to built the GP model. This GP model predicts the SIF values at the other 48 points (a/c is 0.2, 0.4, 1.0, 2.0, a/t is 0.2, 0.5, 0.8, and ϕ is 0.125, 0.375, 0.625, and 0.875) in Table 2 and the prediction values are compared with that of the empirical equations. Figure 8 shows the finite element results listed in Table 2 and the prediction values from GP modeling and the empirical equations.

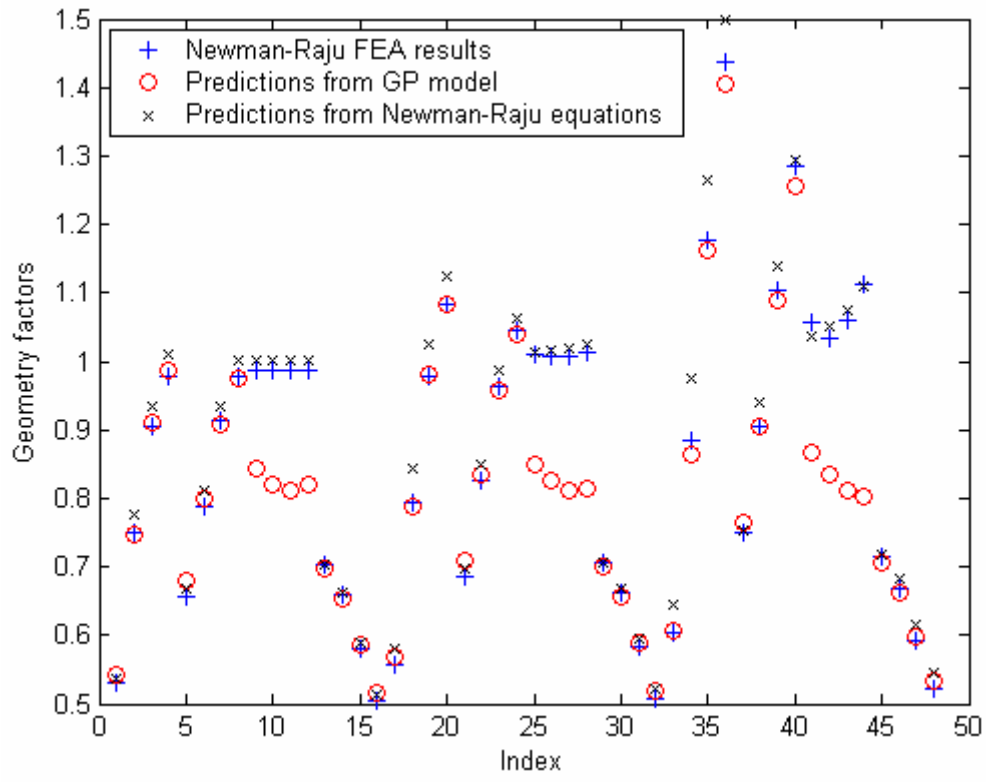

Figure 8 Comparison for embedded elliptical cracks with 27 training points

The average error of GP modeling is:

$$Error = \frac{1}{48}\sum\left|\frac{K_{FEA} - K_{GP}}{K_{FEA}}\right| = 5.72\%$$

The maximum error is 27.96%. The minimum error is 0.06%. The errors at 12 points are greater than 10%, out of 48 validation points.

The average error of the empirical equations is:

$$Error = \frac{1}{48}\sum\left|\frac{K_{FEA} - K_{Eq}}{K_{FEA}}\right| = 2.54\%$$

Then, 36 points (a/c is 0.2, 0.4, 1.0, 2.0, a/t is 0.2, 0.5, 0.8, and ϕ is 0, 0.5, 1) in Table 2 are used as training points. The same 48 points are used for the prediction. Figure 9 shows the finite element results listed in Table 2 and the prediction values from GP modeling and the empirical equations.

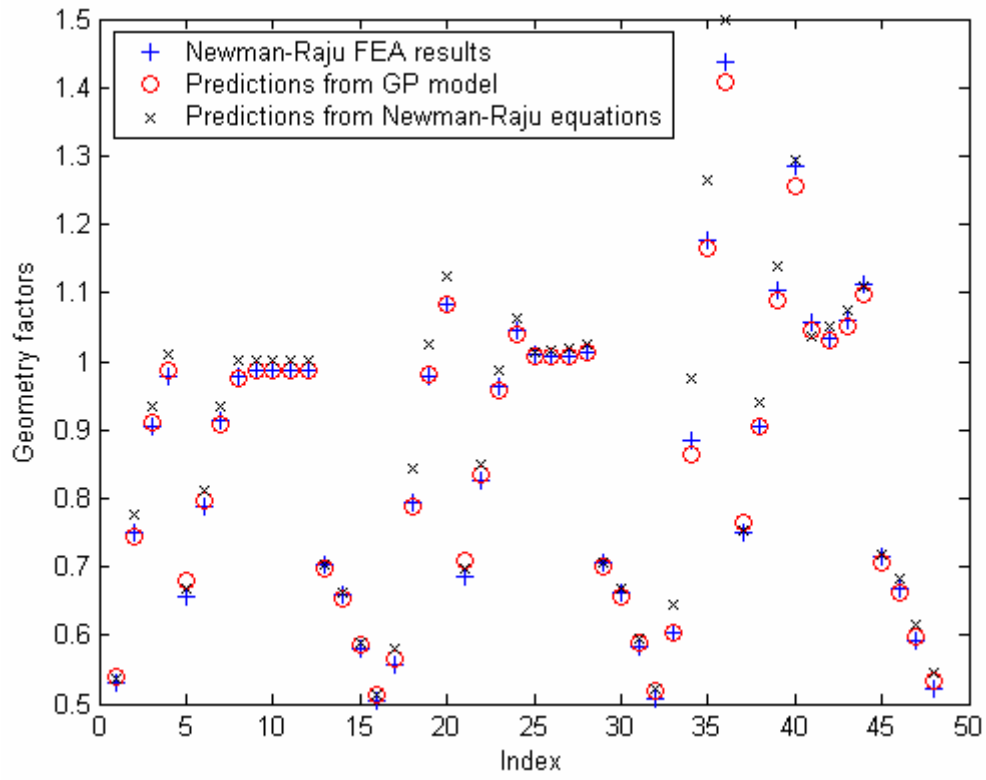

Figure 9 Comparison for embedded elliptical cracks with 36 training points

The average error of GP modeling is:

$$Error = \frac{1}{48}\sum\left|\frac{K_{FEA} - K_{GP}}{K_{FEA}}\right| = 1.02\%$$

The maximum error is 3.51%. The minimum error is 0%.

3.2.4 Quarter-Elliptical Corner Crack

Values of the geometry factor, F_S, obtained from the finite element results for the quarter-elliptic at corner crack in a finite plate subjected to tension are given in Table 3.

Table 3 *Geometry factors F for corner crack* ($c/b \le 0.2; h/b = 1; v = 0.3$)

		a/t		
a/c	**2Φ/π**	**0.2**	**0.5**	**0.8**

	0	0.555	0.761	1.288
	0.125	0.633	0.84	1.34
	0.25	0.753	0.988	1.522
	0.375	0.871	1.141	1.705
0.2	0.5	0.973	1.277	1.85
	0.625	1.055	1.397	2.008
	0.75	1.115	1.495	2.118
	0.875	1.159	1.58	2.263
	1	1.156	1.61	2.45
	0	0.791	0.99	1.397
	0.125	0.774	0.952	1.297
	0.25	0.824	0.997	1.31
	0.375	0.893	1.067	1.346
0.4	0.5	0.964	1.14	1.384
	0.625	1.026	1.21	1.458
	0.75	1.075	1.273	1.528
	0.875	1.117	1.334	1.627
	1	1.132	1.365	1.788
	0	1.162	1.275	1.487
	0.125	1.111	1.207	1.378
	0.25	1.079	1.16	1.29
	0.375	1.064	1.134	1.219
1	0.5	1.059	1.121	1.18
	0.625	1.063	1.123	1.191
	0.75	1.078	1.14	1.231
	0.875	1.109	1.176	1.301

	1	1.159	1.233	1.416
	0	0.8	0.826	0.862
	0.125	0.787	0.811	0.837
	0.25	0.756	0.776	0.793
	0.375	0.722	0.738	0.75
2	0.5	0.683	0.697	0.704
	0.625	0.64	0.653	0.66
	0.75	0.6	0.612	0.624
	0.875	0.579	0.59	0.611
	1	0.586	0.597	0.625

The empirical equations for quarter-elliptical crack are obtained by fitting to the finite elements results presented in Table 3. The equations are:

$$F = [M_1 + M_2(\frac{a}{t})^2 + M_3(\frac{a}{t})^4]g_1 g_2 f_\phi \tag{37}$$

For $a/c \le 1$

$$M_1 = 1.08 - 0.03(\frac{a}{c}) \tag{38}$$

$$M_2 = -0.44 + \frac{1.06}{0.3 + (\frac{a}{c})} \tag{39}$$

$$M_3 = -0.5 + 0.25(\frac{a}{c}) + 14.8(1 - \frac{a}{c})^{15} \tag{40}$$

$$g_1 = 1 + [0.08 + 0.4(\frac{a}{t})^2](1 - \sin\phi)^3 \tag{41}$$

$$g_2 = 1 + [0.08 + 0.15(\frac{a}{t})^2](1 - \cos\phi)^3 \tag{42}$$

and f_ϕ is given by Eq 32.

For $a/c > 1$

$$M_1 = \sqrt{\frac{c}{a}}(1.08 - 0.03\frac{c}{a}) \tag{43}$$

$$M_2 = 0.375(\frac{c}{a})^2 \tag{44}$$

$$M_3 = -0.25(\frac{c}{a})^2 \tag{45}$$

$$g_1 = 1 + [0.08 + 0.4(\frac{c}{t})^2](1 - \sin\phi)^3 \tag{46}$$

$$g_2 = 1 + [0.08 + 0.15(\frac{c}{t})^2](1 - \cos\phi)^3 \tag{47}$$

and f_ϕ is given by Eq 34.

First, 27 points (a/c is 0.2, 0.4, 2.0, a/t is 0.2, 0.5, 0.8, and ϕ is 0, 0.5, 1) in Table 3 are picked as the training points to built the GP model. This GP model is used to predict the SIF values at the other 48 points (a/c is 0.2, 0.4, 1.0, 2.0, a/t is 0.2, 0.5, 0.8, and ϕ is 0.125, 0.375, 0.625, and 0.875) in Table 3 and the prediction values are compared with that of the empirical equations. Figure 10 shows the finite element results listed in Table 3 and the prediction values from GP modeling and the empirical equations.

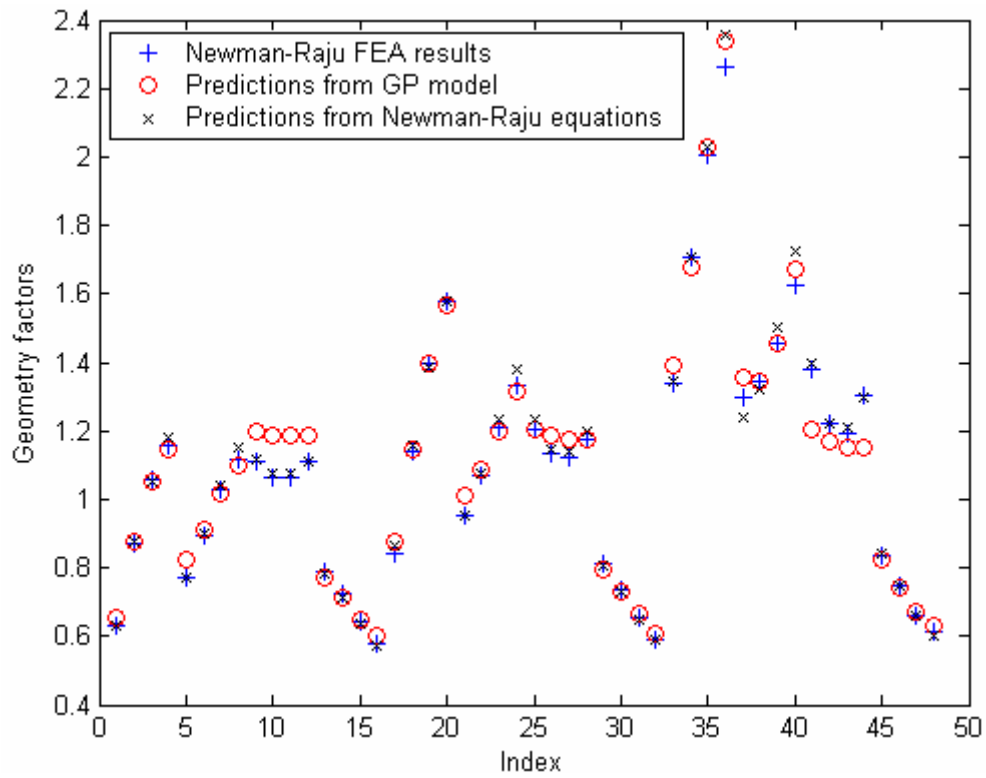

Figure 10 Comparison for quarter-elliptical corner cracks with 27 training points

The average error of GP modeling is:

$$Error = \frac{1}{48}\sum\left|\frac{K_{FEA} - K_{GP}}{K_{FEA}}\right| = 3.16\%$$

The maximum error is 12.8%. The minimum error is 0.05%. The errors at 4 points are greater than 10%, out of 48 validation points.

The average error of the empirical equations is:

$$Error = \frac{1}{48}\sum\left|\frac{K_{FEA} - K_{Eq}}{K_{FEA}}\right| = 1.30\%$$

Next, 36 points (a/c is 0.2, 0.4, 1.0, 2.0, a/t is 0.2, 0.5, 0.8, and ϕ is 0, 0.5, 1) in Table 3 are used as training points. The same 48 points are used for the prediction. Figure

11 shows the finite element results listed in Table 3 and the prediction values from GP modeling and the empirical equations.

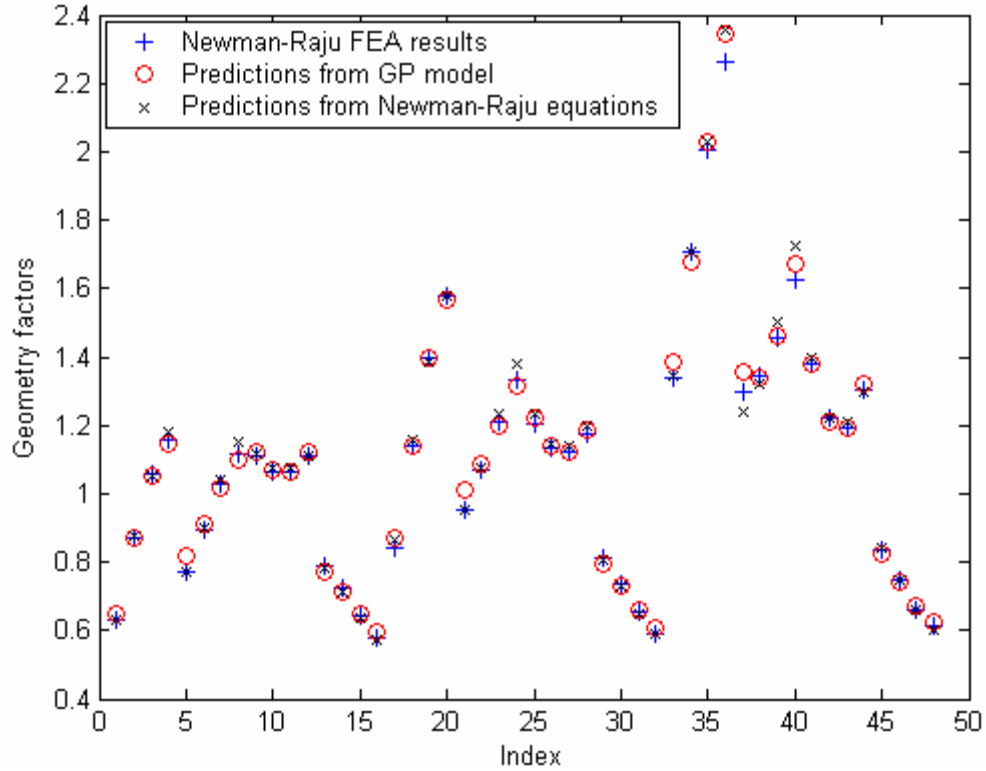

Figure 11 Comparison for quarter-elliptical corner cracks with 36 training points

The average error of GP modeling is:

$$Error = \frac{1}{48}\sum\left|\frac{K_{FEA} - K_{GP}}{K_{FEA}}\right| = 1.57\%$$

The maximum error is 5.98%. The minimum error is 0%.

3.2.5 Semi-Elliptical Surface Crack at Hole

Tables 4 gives the geometry factor values for bi-symmetric semi-elliptical surface cracks emanating from a circular hole in a finite plate for R/t equals 1.

Table 4 *Geometry factors F for surface crack at center of hole in a plate*

$[(R+c)/b \le 0.2; h/b > 1.6; v = 0.3; R/t = 1]$

		a/t		
a/c	**2Φ/π**	**0.2**	**0.5**	**0.8**
	0	0.641	0.607	0.593
	0.125	0.692	0.662	0.643
	0.25	0.836	0.775	0.771
	0.375	1.011	0.905	0.919
	0.5	1.196	1.032	1.094
0.2	0.625	1.405	1.178	1.293
	0.75	1.651	1.362	1.528
	0.833	1.905	1.583	1.765
	0.917	2.179	1.885	2.05
	0.958	2.288	2.121	2.336
	1	1.834	1.958	2.329
	0	1.03	0.872	0.84
	0.125	1.076	0.912	0.872
	0.25	1.202	1.007	0.959
	0.375	1.376	1.131	1.074
	0.5	1.578	1.275	1.234
0.4	0.625	1.804	1.452	1.426
	0.75	2.04	1.667	1.668
	0.833	2.238	1.897	1.914
	0.917	2.396	2.141	2.201
	0.958	2.376	2.255	2.411
	1	1.844	1.923	2.224

	0	2.267	1.806	1.615
	0.125	2.276	1.818	1.619
	0.25	2.301	1.851	1.63
	0.375	2.343	1.905	1.646
	0.5	2.404	1.98	1.73
1	0.625	2.481	2.079	1.852
	0.75	2.566	2.206	2.049
	0.833	2.62	2.321	2.25
	0.917	2.622	2.415	2.452
	0.958	2.468	2.37	2.512
	1	1.95	1.957	2.203
	0	1.944	1.606	1.394
	0.125	1.931	1.6	1.389
	0.25	1.897	1.582	1.377
	0.375	1.84	1.553	1.357
	0.5	1.763	1.514	1.333
2	0.625	1.669	1.468	1.313
	0.75	1.58	1.434	1.31
	0.833	1.498	1.404	1.313
	0.917	1.426	1.387	1.332
	0.958	1.313	1.321	1.294
	1	1.042	1.082	1.077

The empirical stress intensity factor equations for bi-symmetric semielliptical surface cracks at the center of a hole are:

$$F = [M_1 + M_2(\frac{a}{t})^2 + M_3(\frac{a}{t})^4]g_1 g_2 g_3 f_\phi f_w \tag{48}$$

$$f_w = [\sec(\frac{\pi c}{2b})\sec(\frac{\pi(2R+nc)}{4(b-c)+2nc}\sqrt{\frac{a}{t}})]^{1/2} \tag{49}$$

where n = 1 is for a single crack, n = 2 is for bi-symmetric cracks, and the hole is located in the center of the plate.

For $a/c \le 1$

$$M_1 = 1 \tag{50}$$

$$M_2 = \frac{0.05}{0.11 + (\frac{a}{c})^{3/2}} \tag{51}$$

$$M_3 = \frac{0.29}{0.23 + (\frac{a}{c})^{3/2}} \tag{52}$$

$$g_1 = 1 - \frac{(\frac{a}{t})^4}{1 + 4(\frac{a}{c})}\cos\phi \tag{53}$$

$$g_2 = \frac{1 + 0.358\lambda + 1.425\lambda^2 - 1.578\lambda^3 + 2.156\lambda^4}{1 + 0.08\lambda^2} \tag{54}$$

where

$$\lambda = \frac{1}{1 + \frac{c}{R}\cos(0.9\phi)} \tag{55}$$

$$g_3 = 1 + 0.1(1 - \cos\phi)^2(1 - \frac{a}{t})^{10} \tag{56}$$

and f_ϕ is given by Eq 32.

For $a/c > 1$

$$M_1 = \sqrt{\frac{c}{a}} \tag{57}$$

The functions M_2, M_3, g_1, g_2, g_3 and λ are given by Eqs 51 through 55 and the functions f_ϕ is given by Eq 34.

First, 45 points (a/c is 0.2, 0.4, 2.0, a/t is 0.2, 0.5, 0.8, and ϕ is 0, 0.25, 0.5, 0.75, 1) in Table 4 are picked as the training points to built the GP model. This GP model is used to predict the SIF values at the other 48 points (a/c is 0.2, 0.4, 1.0, 2.0, a/t is 0.2, 0.5, 0.8, and ϕ is 0.125, 0.375, 0.625, and 0.875) in Table 4 and the prediction values are compared with that of the empirical equations. Figure 12 shows the finite element results listed in Table 4 and the prediction values from GP modeling and the empirical equations.

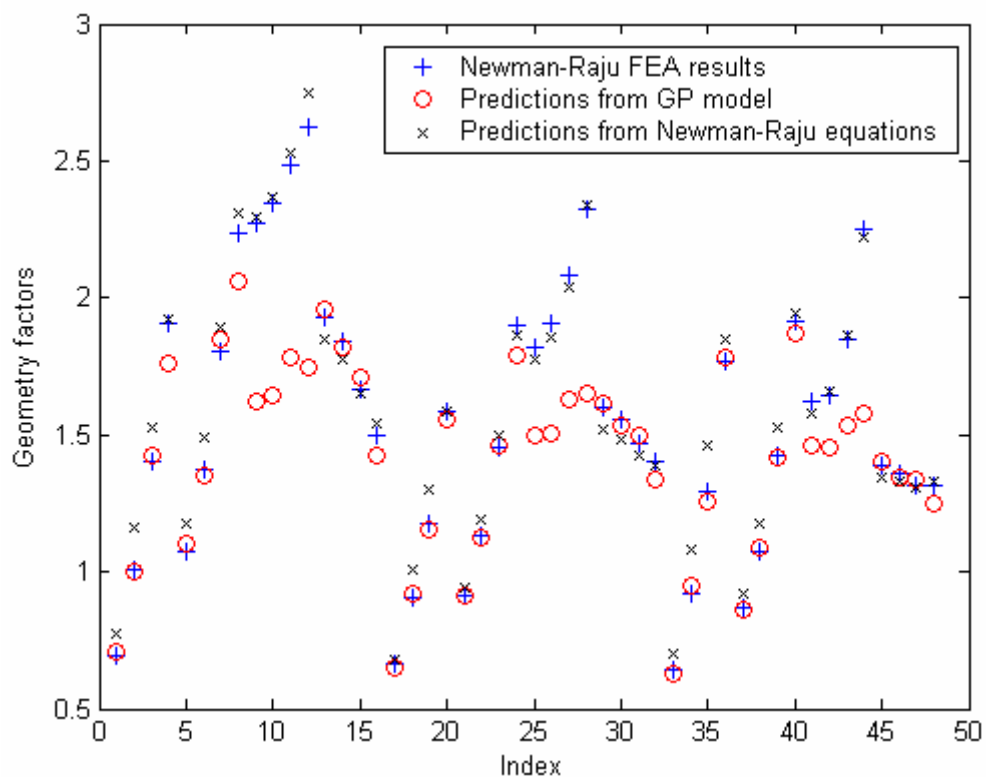

Figure 12 Comparison for semi-elliptical surface cracks at hole with 45 training points

The average error of GP modeling is:

$$Error = \frac{1}{48}\sum\left|\frac{K_{FEA} - K_{GP}}{K_{FEA}}\right| = 7.57\%$$

The maximum error is 33.29%. The minimum error is 0.04%. The errors at 11 points are greater than 10%, out of 48 validation points.

The average error of the empirical equations is:

$$Error = \frac{1}{48}\sum\left|\frac{K_{FEA} - K_{Eq}}{K_{FEA}}\right| = 4.64\%$$

Then, 60 points (a/c is 0.2, 0.4, 1.0, 2.0, a/t is 0.2, 0.5, 0.8, and ϕ is 0, 0.25, 0.5, 0.75, 1) in Table 4 are used as training points. The same 48 points are used for the prediction. Figure 13 shows the finite element results listed in Table 4 and the prediction values from GP modeling and the empirical equations.

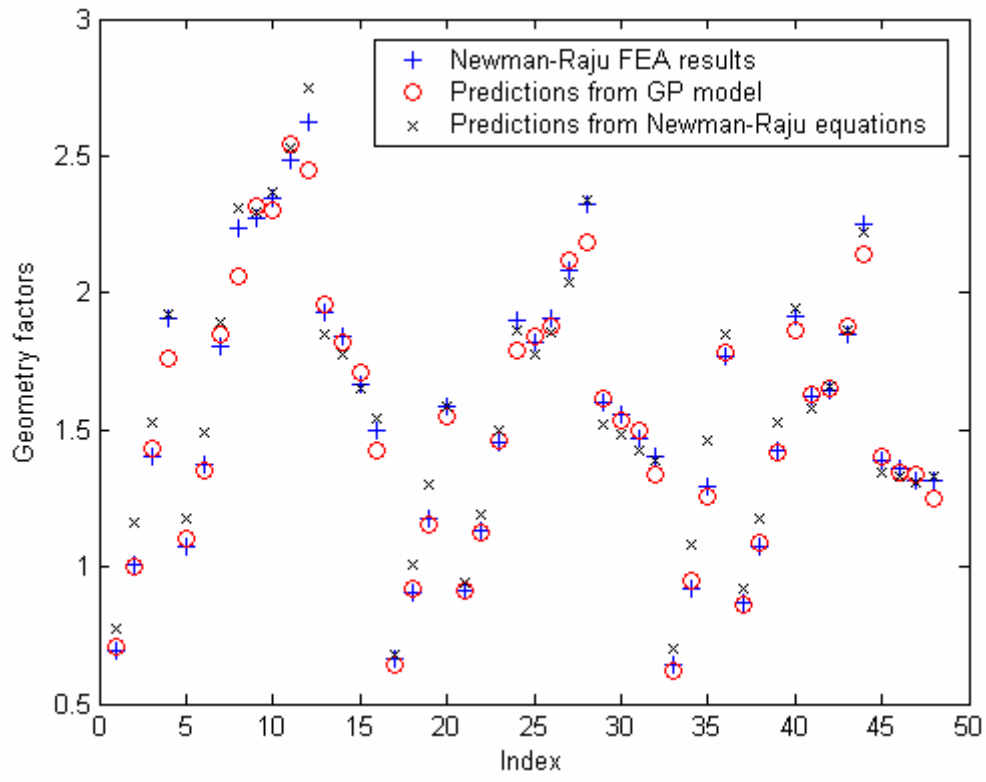

Figure 13 Comparison for semi-elliptical surface cracks at hole with 60 training points

The average error of GP modeling is:

$$Error = \frac{1}{48}\sum\left|\frac{K_{FEA} - K_{GP}}{K_{FEA}}\right| = 2.41\%$$

The maximum error is 7.95%. The minimum error is 0.002%.

Table 5 lists the errors for all the cases with different numbers of training points.

Table 5 *The average error of various cracks with different numbers of training points*

Type	GP		Empirical equations	
	# of training points	Error (%)	# of training points	Error (%)
Semi-elliptical surface crack	27	4.36	180	2.61
	36	1.64		
	60	1.17		
Embedded elliptical crack	27	5.72	108	2.38
	36	1.02		
Quarter-elliptical corner crack	27	3.16	108	1.3
	36	1.57		
Semi-elliptical surface crack at hole	45	7.57	132	4.64
	60	2.41		

3.2.6 Life prediction of Semi-Elliptical Surface Crack

GP modeling is applied to life prediction in this section. The initial crack depth a_0, the final crack depth a_f, the initial crack length c_0, the final crack length c_f, the width of the plate *b* and the thickness *t* are the configuration parameters. The external loading is σ and *c* and *m* are two fatigue parameters used in crack propagation. Table 6 presents the values of the parameters.

Table 6 *Values of all the parameters*

Parameters	Value	Parameters	Value
a_0	0.2 mm	c_0	0.2 mm
a_f	0.8 mm	c_f	4 mm
t	1 mm	b	8 mm
H	8 mm	σ	25 Mpa
c	3.667	m	3.11e-10

Paris law is used to calculate the crack growth rate, which is expressed as:

$$a_{N+1} = a_N + \Delta a \tag{58}$$

$$\Delta a = \frac{da}{dn} = c(\Delta k(a_N, F))^m \tag{59}$$

Figure 14 shows the results of life prediction using GP modeling and the Newman – Raju empirical equations.

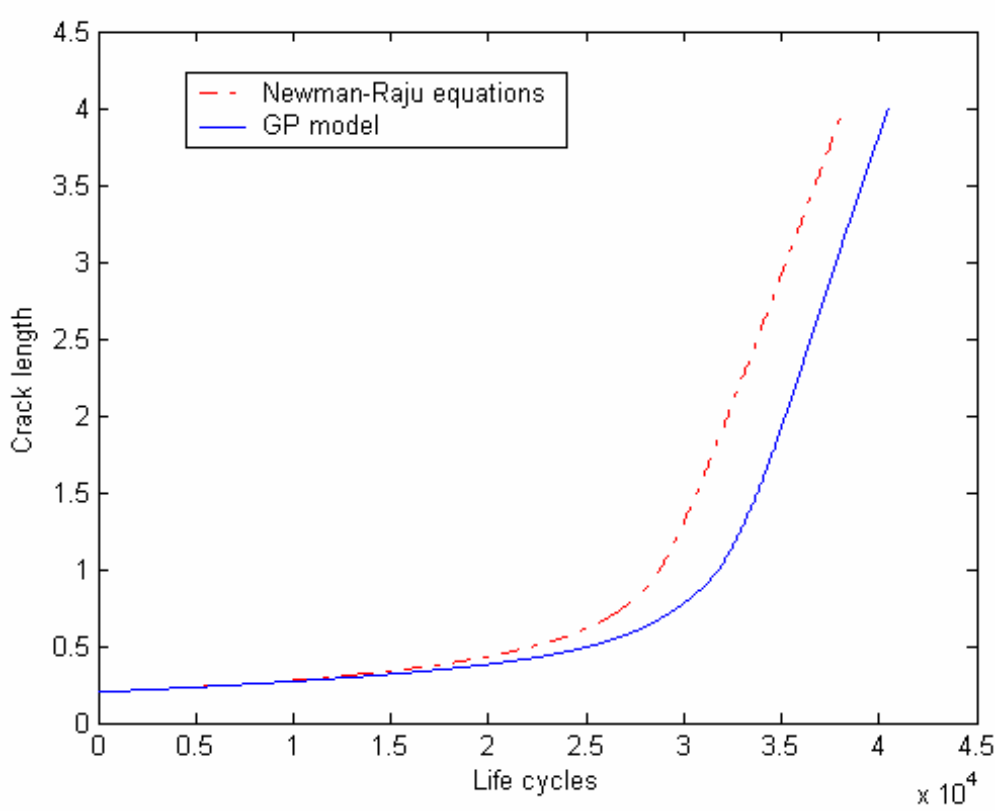

Figure 14 Life prediction using GP modeling and Newman's equations

The number of life cycles to reach the final crack length c_f using Newman's empirical equations is:

$$N_{Eq} = 38032$$

The number of life cycles to reach the final crack length c_f with using the GP model is:

$$N_{GP} = 40506$$

The example demonstrates the use of the GP model in fatigue life prediction expressed as the number of life cycles. The result shows that the difference in the number of life cycles estimated through the empirical equations and the GP model is about 6%. The purpose of the example used here is to develop a proof of concept in relation to life

prediction using the GP model. An extension to the present study can include more realistic examples.

3.3 Conclusion

From Table 5, it is found that GP modeling can reach the same level of accuracy as the Newman-Raju empirical model with much less training points, thus saving considerable computational effort. GP modeling successfully captures the highly complex relationship between input and output variables with a small number of training points. The life prediction using the GP model is also close to the result using the Newman-Raju empirical equations. The application of Gaussian process modeling to the examples of three dimensional cracks in this chapter demonstrates the accuracy and efficiency of the method. Furthermore, given the difficulty of selecting a proper form in traditional response surface methods, GP modeling is easily applicable to any problem without assuming any explicit form.

CHAPTER IV

APPLICATION TO RAILROAD WHEEL FATIGUE CRACK GROWTH

4.1 Introduction

The fatigue problem of railroad wheels, referred to as rolling contact fatigue [16], is caused by repeated contact stress during the rolling motion. An overview of the rolling contact fatigue problem is given in [17]. Elliptical cracks of various sizes are considered below the tread surface. Since the problem is mixed-mode, the range of equivalent stress intensity factor, ΔK_{eq}, at the crack tip is calculated using the uni-modal stress intensity factor values obtained from a mixed-mode crack growth model based on critical plane concepts [18]. The ΔK_{eq} at the crack tip depends on several parameters such as, the detected crack size, crack location, symmetric/unsymmetric crack growth, rail-wheel contact location, wheel diameter, and the applied load.

Obviously, to investigate all the effects of the above mentioned parameters through finite element analysis is very time consuming. A response surface method is necessary to reduce the computational effort. In this chapter, Gaussian process modeling is applied to this problem because of its efficiency and accuracy. The crack size and applied load are the two parameters to be considered. Finite element analysis is used to generate the data set for both training and testing points. The comparison of Gaussian process modeling and other response surface methods such as polynomial expansion is also done.

4.2 Wheel Model

4.2.1 Finite element model

A three-dimensional finite element model is used in this paper. This finite element model considers both material and geometric nonlinearities and predicts the stress response in the contact region. A sub-model is cut from the full model focusing on the contact region and built using the same type of elements that are used for the full model. Figure 1 shows both the full model and sub-model.

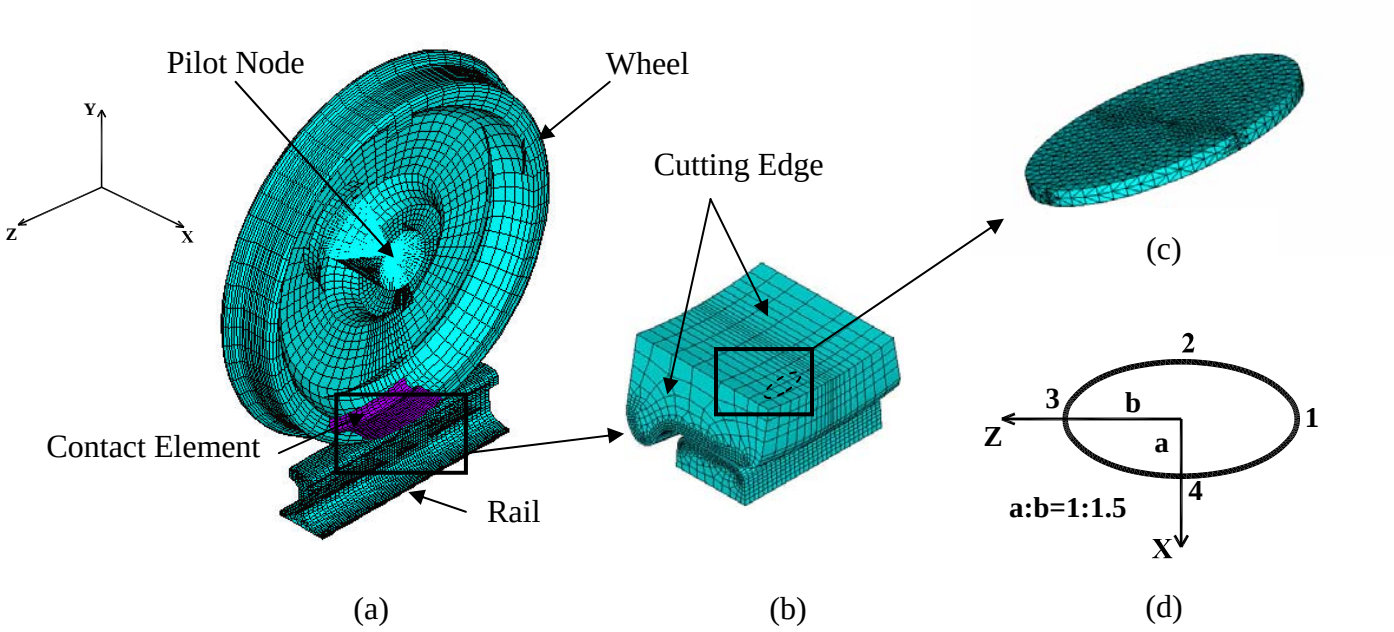

Fig.15 Finite element model of railroad wheel: (a) Full model, (b) Sub-model, (c) crack, (d) crack

4.2.2 Mixed mode crack growth model

Liu and Mahadevan [18] developed critical plane-based mixed-mode fatigue crack growth rate. The general crack propagation equation is expressed as

$$\Delta K_{eq} = \frac{1}{B}\sqrt{(\Delta k_1)^2 + (\frac{\Delta k_2}{s})^2 + (\frac{\Delta k_3}{s})^2 + A(\frac{\Delta k^H}{s})^2} \qquad (60)$$

$$\text{and } \frac{da}{dn} = f(\Delta k_{eq})$$

where ΔK_{eq} is the equivalent stress intensity factor range under mixed-mode loading. $f()$ is the crack growth curve ($\frac{da}{dN}$ vs. Δk) obtained under mode I loading. Δk_1, Δk_2, Δk_3 and Δk^H are the loading parameters with the same unit as the stress intensity factor. a is the half length of the crack. The subscripts 1, 2, 3 indicate the directions of the stress amplitude as shown in Fig. 16. The superscript *H* indicates the hydrostatic stress related term. *s* is the ratio of Mode II and Mode I stress intensity factors under a specific crack growth rate (*da/dN*). *A* and *B* are material parameters and are listed in Table. 7.

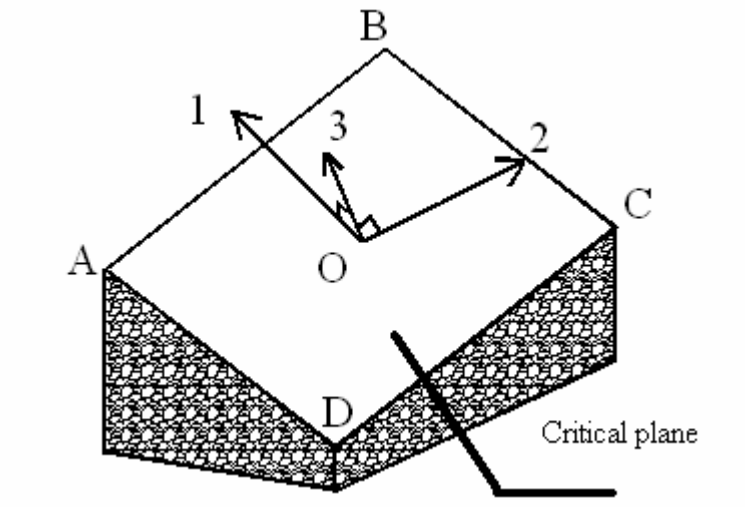

Figure 16 Schematic illustration of stress components on the critical plane

The critical plane is defined as the material plane which has an angle of γ away from the maximum normal stress amplitude plane. α is the critical plane orientation. It can be expressed as

$$\alpha = \beta + \gamma \tag{61}$$

where β is the maximum normal stress amplitude plane orientation at the far field. γ is defined in Table 7. For general non-proportional loading, the axial loading and the torsional loading may not reach their maxima simultaneously. Numerical search is required to find the value of β, k_1, k_2, k_3 and k^H [18]. Eqs. (60) and (61) together with the material parameters defined in Table 7 are used for fatigue crack growth rate prediction under general mixed-mode loading

Table 7 *Material parameters for fatigue crack propagation prediction*

Material Property	$s = \frac{K_{II,da/dN}}{K_{I,da/dN}} < 1$	$s = \frac{K_{II,da/dN}}{K_{I,da/dN}} \geq 1$
γ	$cos(2\gamma) = \frac{-2 + \sqrt{4 - 4(1/s^2 - 3)(5 - 1/s^2 - 4s^2)}}{2(5 - 1/s^2 - 4s^2)}$	$\gamma = 0$
A	$A = 0$	$A = 9(s^2 - 1)$
B	$B = [cos^2(2\gamma)s^2 + sin^2(2\gamma)]^{\frac{1}{2}}$	$B = s$

As shown in Liu and Mahadevan [18], the ratio of mode II and mode I fatigue crack threshold stress intensity factors $s = \frac{K_{II,th}}{K_{I,th}}$ relates to different material failure mechanisms. A larger value of s ($s > 1$) indicates tensile dominated failure and a smaller value of s ($s = \frac{1}{\sqrt{3}}$) indicates shear dominated failure. If the value of s is known, the proposed model can automatically adapt for different failure mechanisms.

The stress intensity factors obtained from finite element analysis and the mixed-mode crack propagation model are combined together to calculate the equivalent stress intensity factor at the crack tip as in Eq. (60).

4.2.3 Finite element results

As mentioned above, the crack size and applied load are the two parameters to be considered here. In this study, both of the two parameters are divided into 5 segments. The crack size is 0.3, 0.6, 1, 2, 3 mm, respectively. The applied load is 58.48, 102.34, 146.2, 175.44, 219.3 KN (the applied load is equal to load factor multiplying146.2KN and the load factor is 0.4, 0.7, 1, 1.2, 1.5 respectively). So there are totally 25 points in the data set. 9 of 25 points are used as training points to construct GP modeling and other response surfaces and the other 16 points are used as testing points. Table 8 and Table 9 list the training points and testing points respectively.

Table 8 *Training points for the problem of railroad wheel*

Load factor	crack size (mm)	SIF (Mpa $\sqrt{m}$)
0.4	0.3	0.544769
0.4	1	0.700043
0.4	3	1.768284
1	0.3	1.822575
1	1	2.609908
1	3	5.865713
1.5	0.3	2.700879
1.5	1	3.894887

1.5	3	9.047153

Table 9 *Testing points for the problem of railroad wheel*

Load factor	crack size (mm)	SIF (Mpa$\sqrt{m}$)
0.4	0.6	0.694926
0.4	2	1.143716
0.7	0.3	1.154115
0.7	0.6	1.455873
0.7	1	1.699882
0.7	2	2.813124
0.7	3	4.142482
1	0.6	2.275431
1	2	4.115527
1.2	0.3	2.159722
1.2	0.6	2.775047
1.2	1	3.29081
1.2	2	4.973068
1.2	3	6.956697
1.5	0.6	2.867027
1.5	2	6.08698

4.2.4 Comparison of response surface methodologies

Three types of response surfaces are compared here, which are as follows:

1) GP modeling

2) Polynomial expansion

$$y = \beta_0 + \beta_1 * a + \beta_2 * a^2 + \beta_3 * F + \beta_4 * F^2 \tag{62}$$

where *a* is crack size and *F* is the load factor. $\beta_0 \sim \beta_4$ are the coefficients obtained from least square estimation.

3) Nonlinear regression

$$y = \beta_0 + \beta_1 * F * \sqrt{a} \tag{63}$$

where *a* is crack size and *F* is the load factor. β_0 and β_1 are the coefficients obtained from least square estimation. The reason for using this regression model is that in linear fracture mechanics, SIF can be expressed as:

$$K_I = \sigma\sqrt{\pi a} F_S \tag{64}$$

where *a* is the crack depth, σ is the external loading and F_S is the geometry factor. $\sigma\sqrt{a}$ is modeled by the variable $F\sqrt{a}$ in the regression.

All the response surfaces are constructed using the same 9 training points. The prediction values from the three response surfaces are compared with true values obtained from finite element analysis in Table 9 to check the accuracy. The results are listed in Table 10.

Table 10 *Comparison of various response surfaces*

RSM	# of training points	Average error* (%)	R square
GP modeling	9	5.4	1
Polynomial Expansion	9	12.73	0.877

Nonlinear Regression	9	23.88	0.9735

*Error = $\frac{1}{n}\sum\frac{\left|K_{FEA}-K_{prediction}\right|}{K_{FEA}}$ and n is the number of testing points.

The results show that although the R square values of the other response surfaces are high, the errors are still much larger than GP modeling. Both are greater than 10% while the error of GP modeling is about 5%. So the polynomial expansion and nonlinear regression fail to capture the relationship between the input and output variables.

4.3 Conclusion

From Table 10, it is found that GP modeling is more accurate than other models with the same number of training points. Although the R square values are very high, the prediction values from other models are still not satisfactory. It is possible that if the relationship between inputs and outputs was complicated by considering more variables, the prediction values would be much less accurate. The reason for this problem may be the form of response surface methods. With the increasing complexity of problems, more proper forms have to be selected if traditional methods are used here. As a non-parametric method, the GP model can overcome the problem of selecting the form of the surrogate model.

CHAPTER V

APPLICATION TO FATIGUE CRACK GROWTH DATA

5.1 Introduction

As pointed out by Virkler [19], metal fatigue is a stochastic phenomenon. The scatter in fatigue data is due to the inhomogeneity of the material instead of the experiment inaccuracies. Generally, the material is assumed to be homogeneous at the macroscopic level. However, it is not homogeneous at the microscopic level. As shown in Figure 17, the crack growth rate varies with the stress intensity factor ΔK and the statistical variability also changes with ΔK . In order to statistically characterize the random crack growth rate, it is helpful to calculate the distribution of the crack growth rate from experimental data.

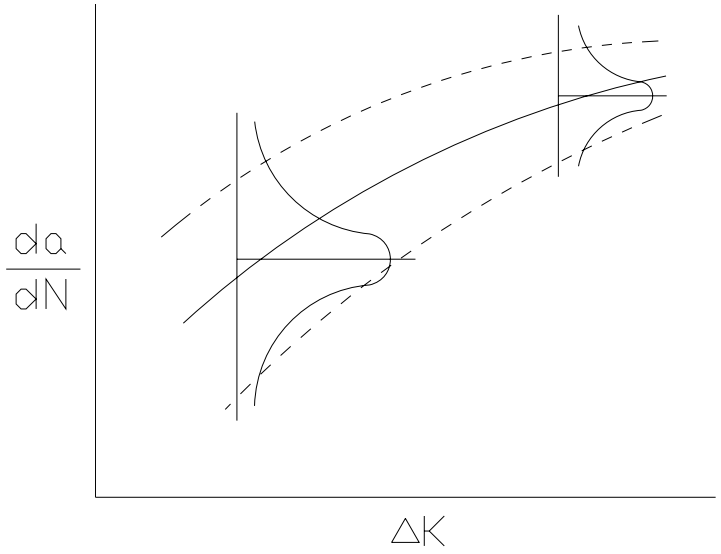

Figure 17 Distribution of *da/dn*

Since GP modeling can give not only the estimated values (mean value) but also the uncertainty (variance) at the untested points, we shall apply it to fit the experimental data and capture the random behavior in fatigue data.

5.2 Greedy point selection

Since GP modeling can provide not only the estimate value (mean value) but also the uncertainty (variance) at any prediction location. The location where the uncertainty is large implies that there is a lack of training points in that region. So the estimate value there may be less accurate.

The basic idea of greedy point selection is to build the GP model with a few training points (2 or 3), calculate the predictions at other locations and then improve the model by adding a training point where the variance is highest. The procedure repeats until the target level of variance is reached. This assures that each new training point is the most necessary one in the model.

5.3 Model validation

The method is validated by fatigue experimental data of 2024 T3 aluminum alloy and 7075 t651 aluminum alloy. In the first numerical example, GP modeling is applied to data of 2024 T3 aluminum alloy. There are three R ratios in the fatigue data. The R ratios are 0, 0.5, and 0.7 respectively. Figure 18 shows the data of fatigue crack growth rate versus stress intensity factor.

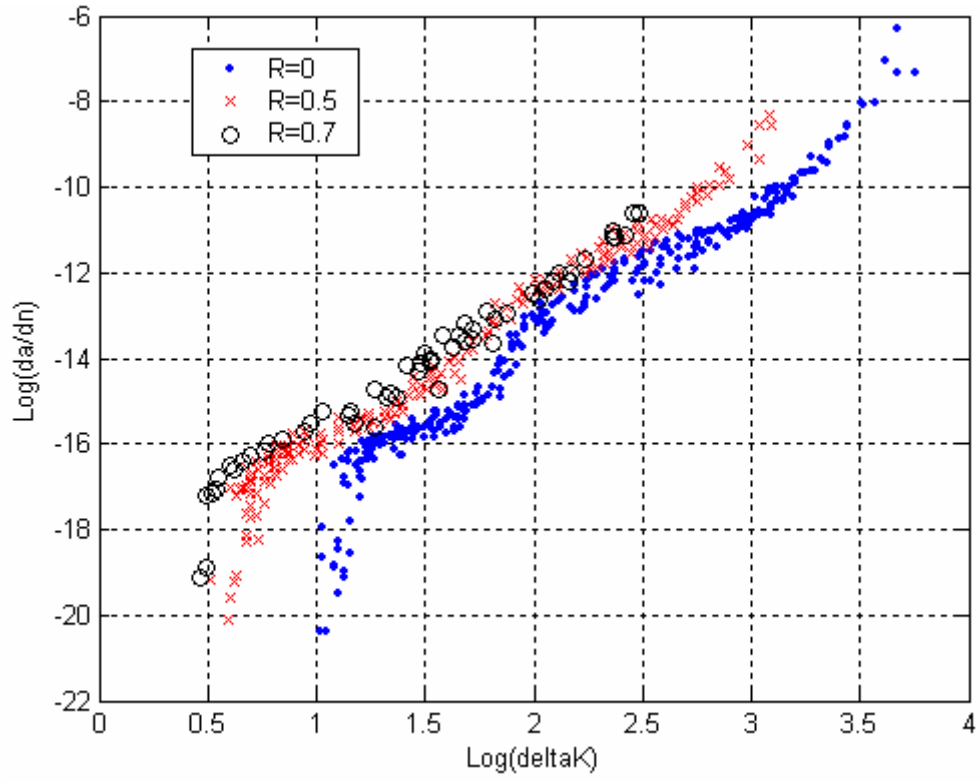

Figure 18 Fatigue data of 2024 T3 aluminum alloy

First, GP modeling is applied to the case of R = 0. In this case, GP modeling is used to capture the relationship between stress intensity factor and crack growth rate (da/dn). The relationship between two random variables can be expressed as follows:

$$\frac{da}{dn} = f(\Delta K) \tag{65}$$

44 points are selected as training points to build GP modeling. Figure 19 shows all the training points and Figure 20 shows the model prediction. The average error between the prediction values and experimental data is 2.83%. The maximum error is 12.8%. The minimum error is 0.5%. The errors at 18 points are greater than 10%, out of 247 (= 291- 44) validation points.

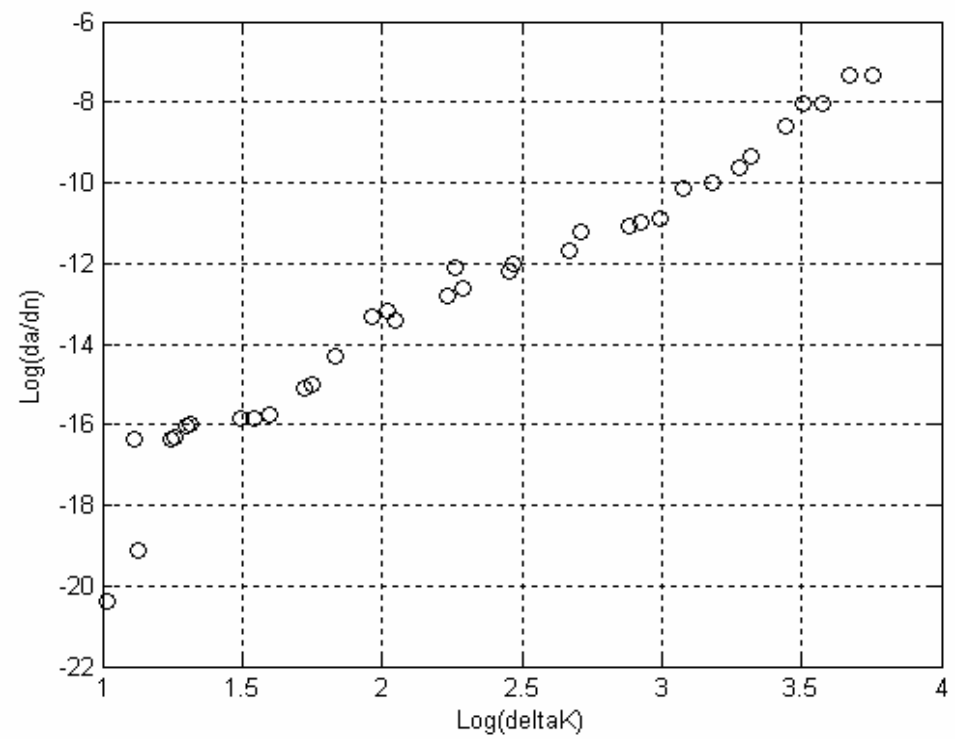

Figure 19 Training points for the fatigue data with R = 0

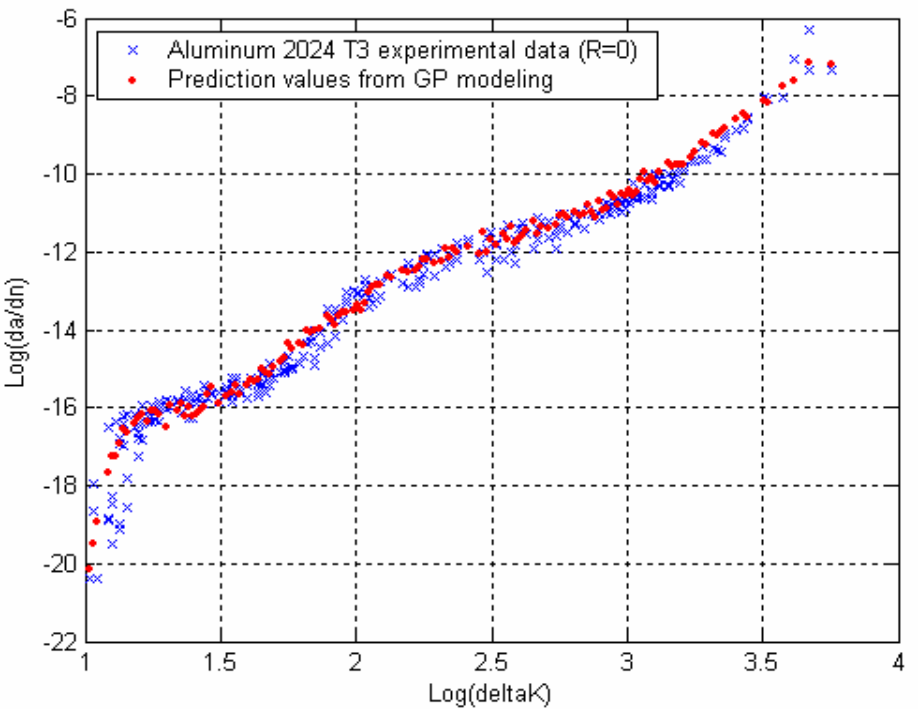

Figure 20 Comparison between fatigue data and model prediction (R = 0)

Second, GP modeling is applied to the entire data set including the three *R* ratios. In this case, GP modeling is used to capture the relationship between stress intensity factor, *R* ratio and crack growth rate (da/dn). The relationship can be expressed as follows:

$$\frac{da}{dn} = f(\Delta K, R) \tag{66}$$

37 points are selected as training points to build GP modeling. Figure 214 shows all the training points and Figure 22 shows the model prediction. The average error between the prediction values and experimental data is 3.19%. The maximum error is 19.35%. The minimum error is 0.3%. The errors at 14 points are greater than 10%, out of 492 (= 529 – 37) validation points.

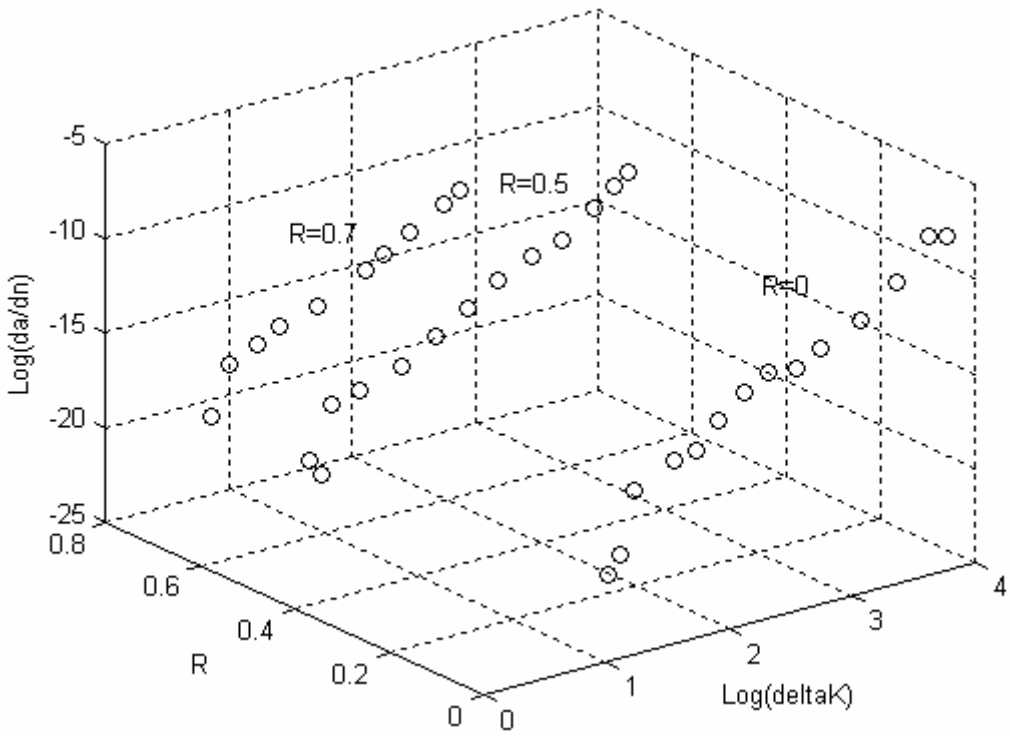

Figure 21 Training points for the whole fatigue data including three *R* ratios

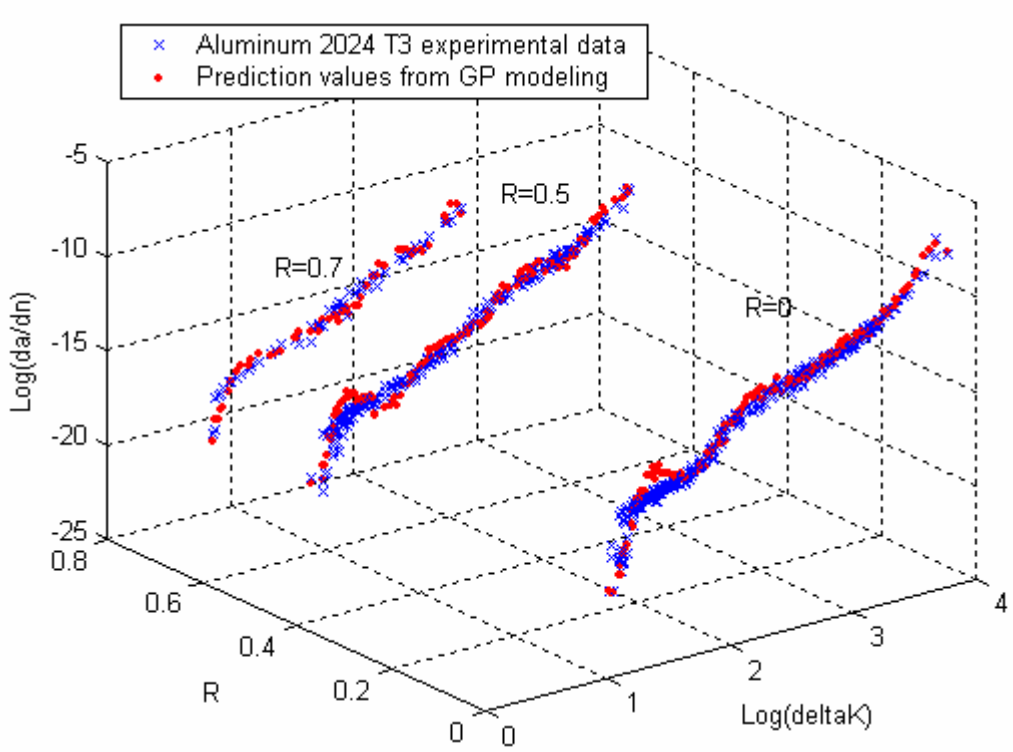

Figure 22 Comparison between fatigue data and model prediction (R = 0, 0.5, 0.7)

In the second example, GP modeling is applied to data of 7075 t651 aluminum alloy. The *R* ratios are 0.01, 0.1, 0.33, and 0.75 respectively. Figure 23 shows the data of fatigue crack growth rate versus stress intensity factor.

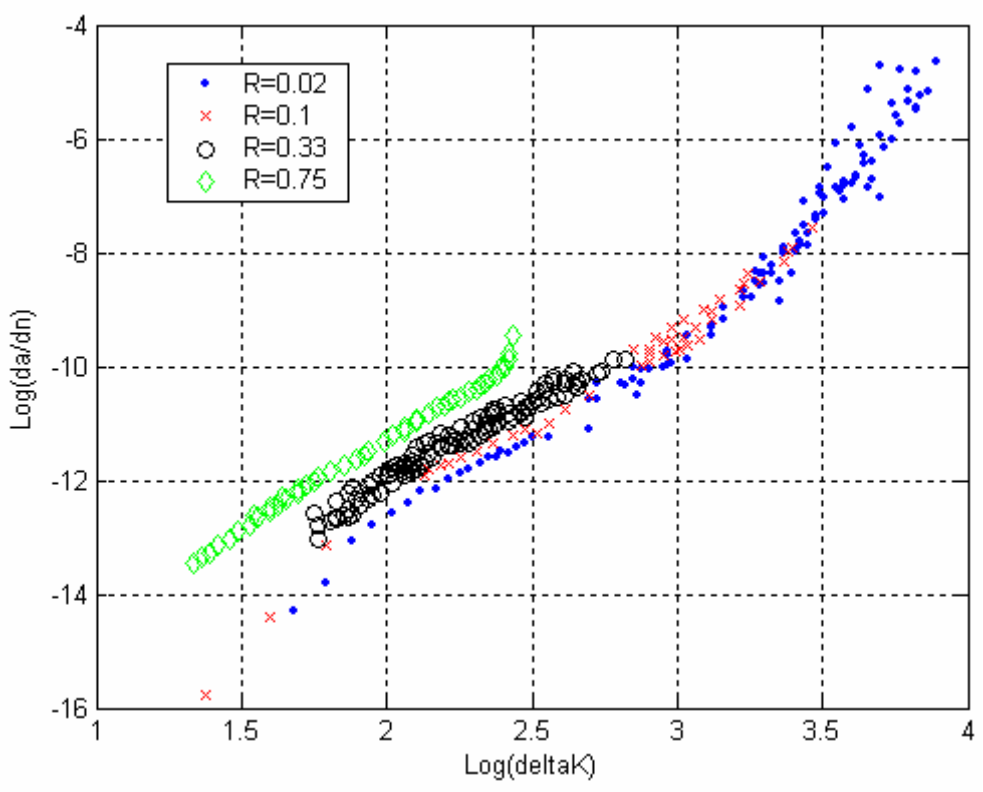

Figure 23 Fatigue data of 7075 T651 aluminum alloy

First, GP modeling is applied to the case of R = 0.02. 7 points are selected as training points to build GP modeling. Figure 24 shows all the training points and Figure 25 shows the model prediction. The average error between the prediction values and experimental data is 3.56%. The maximum error is 23.5%. The minimum error is 0.3%. The errors at 9 points are greater than 10%, out of 106 (= 113 – 7) validation points.

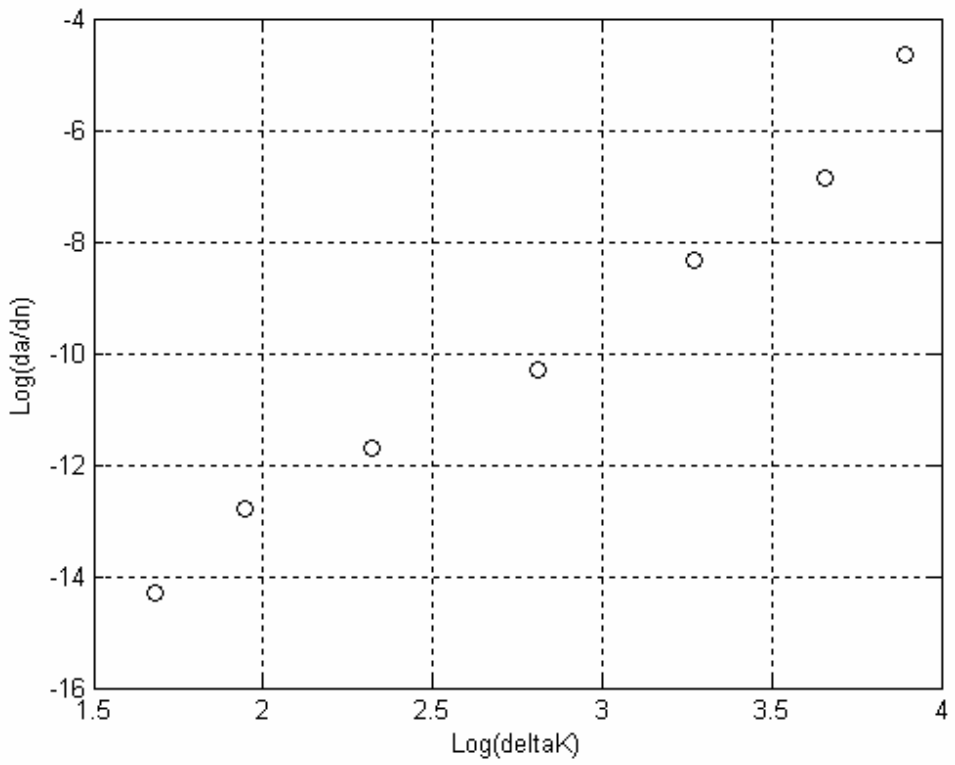

Figure 24 Training points for the fatigue data with R = 0.02

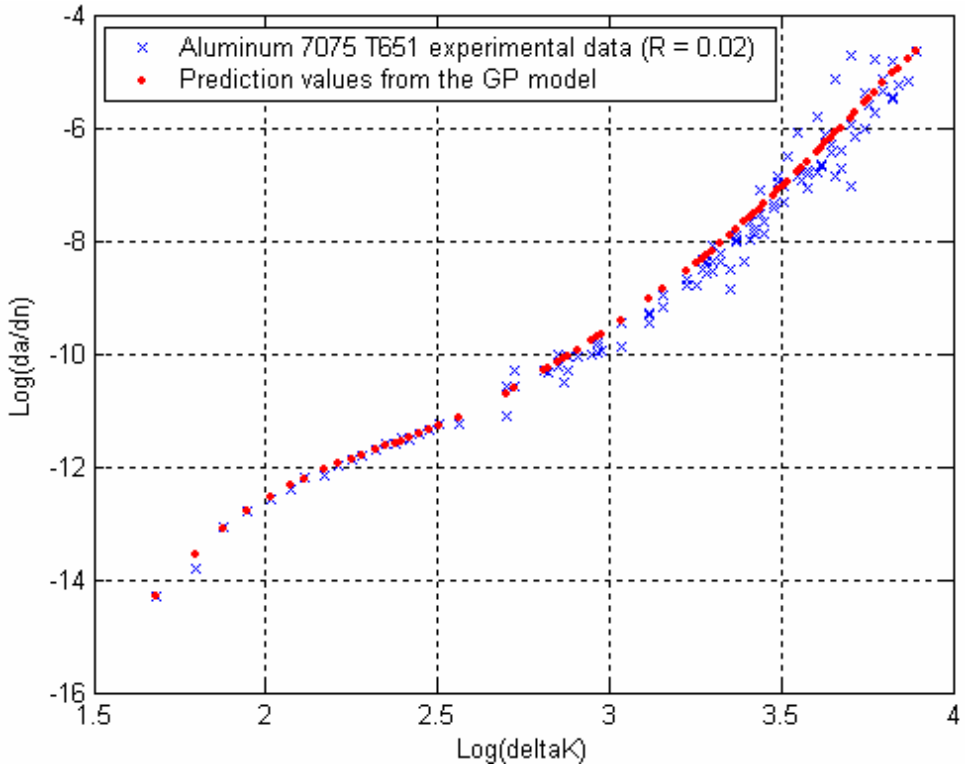

Figure 25 Comparison between fatigue data and model prediction (R = 0.02)

Then, GP modeling is applied to the whole data set including the four *R* ratios. 16 points are selected as training points to build GP modeling. Figure 26 shows all the training points and Figure 27 shows the model prediction. The average error between the prediction values and experimental data is 2.27%. The maximum error is 27.36%. The minimum error is 0.4%. The errors at 7 points are greater than 10%, out of 295 (= 311 – 16) validation points.

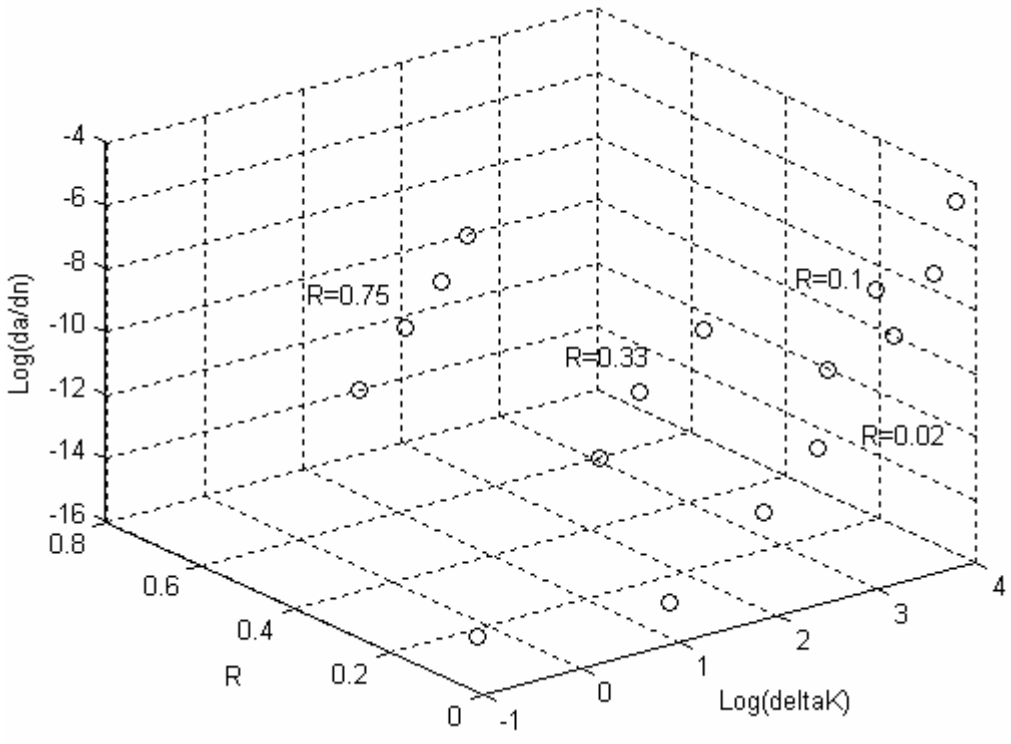

Figure 26 Training points for the whole fatigue data including four *R* ratios

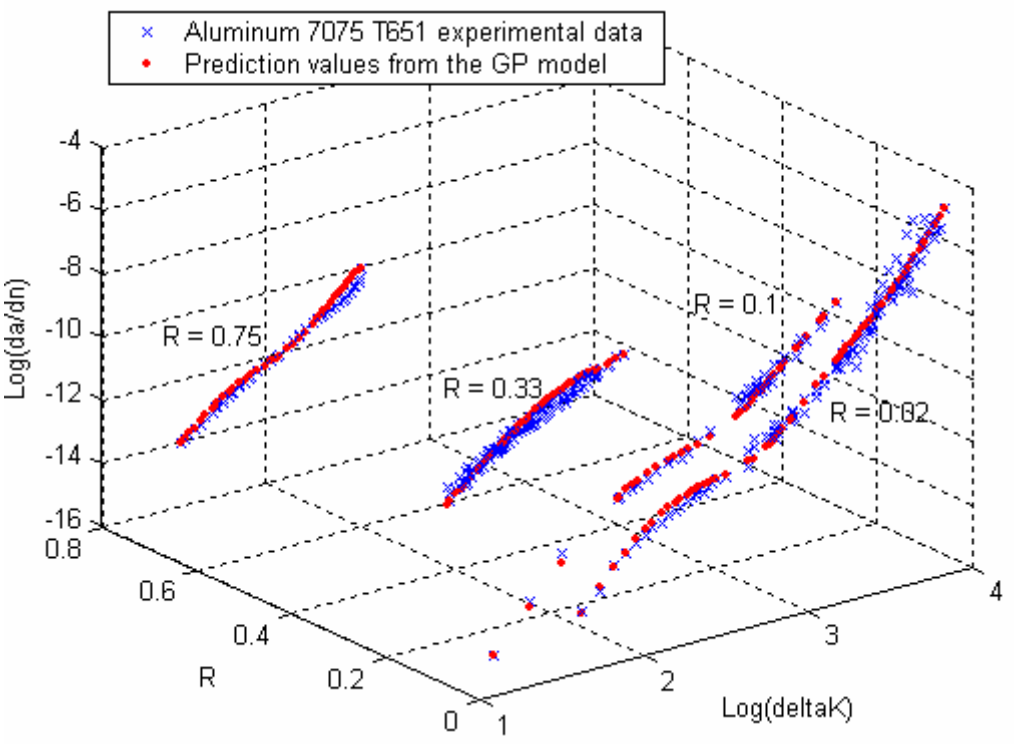

Figure 27 Comparison between fatigue data and model prediction (R = 0.02, 0.1, 0.33, and 0.75)

5.4 Conclusion

This chapter presents the use of Gaussian process modeling of stochastic fatigue crack growth data. Stress intensity factor and other factors are modeled as input variables and fatigue crack growth rate is modeled as the output variable. The results show that the model can capture the scatter phenomenon of fatigue data well with a few training points. With the greedy point selection method, training points are selected where most uncertainty is observed. In general, the number of training points ranges from 10 to about 40, and the average error is typically about 3% or less. This implies that combining GP modeling and greedy point selection with fatigue testing will significantly reduce the cost of fatigue testing.

CHAPTER VI

CONCLUSION AND FUTURE WORK

6.1 Summary of contribution

Finite element analysis is used to calculate the values of stress intensity factors in linear fracture mechanics analysis of realistic structures. Since it is very time consuming, a response surface is needed to approximate the relationship between input and output variables and to save the computational effort. This study proposed a Gaussian process response surface approach to address the problem with more accuracy and efficiency. Gaussian process modeling is powerful in capturing the complex relationship between input and output variables. In the present study, stress intensity factor is modeled as output variable and other factors including geometry, loading, and material properties are modeled as input variables, and the finite element computation of stress intensity factor is replaced by a Gaussian process surrogate model.

The scatter phenomenon in fatigue data is also modeled with this approach. Since Gaussian process modeling gives not only the estimated values but also the uncertainty at untested points, a greedy point selection method is used to select training points where most uncertainty is observed. The results imply that combining GP modeling and greedy point selection can significantly reduce the fatigue testing cost in characterizing the statistical nature of fatigue crack growth data.

6.2 Future work

The advantages of GP modeling, which are to save computational effort and fatigue test effort, have been demonstrated so far. Next, this method needs to be applied to realistic problems. In realistic problems, various aspects including variable amplitude loading, complicated geometry, and different types of crack need to be taken into consideration. Given many factors to be considered, GP modeling approach has the potential to provide a good surrogate model to capture the input – output relationships. In building the GP model, design of experiment needs to be implemented carefully and accurate finite element models are also necessary.

REFERENCES

1. W. K. Liu and T. Belytschko, *Computational Mechanics of Probabilistic and Reliability Analysis*. Elme Press International (1989).

2. W. K. Liu, G. H. Besterfield and T. Belytschko, *Variational approach to probabilistic finite elements. J. Engng Mech. ASCE* 114, 2115-2133 (1988).

3. H. H. Harkness, T. Belytschko and W. K. Liu, Finite-element reliability-analysis of fatigue life. *Nuclear Engng Design* 113, 314-320 (1992).

4. A. Der Kiureghian and B.-J. Ke, The stochastic finite element method in structural reliability. *Probabilistic Engng Mech.* 3, 83-91 (1988).

5. L. Faravelli, Response surface approach for reliability analysis. *J. Engng Mech. ASME* 115, 2763-2781 (1989).

6. L. Faravelli, A response surface approach for reliability analysis. *RILEM Symp. Stoch. Meth. Mater. Struct. Engng* (1986).

7. Newman, J. C. and Raju, I. S., "Stress-Intensity Factor Equations for Cracks in Three-Dimensional Finite Bodies," *Fracture Mechanics*: Fourteen Symposium-Volume I: Theory and Analysis, ASTM STP 791, J. C. Lewis and G. Shines, Eds., American Society for Testing and Materials, 1983, pp. I-238-I-265

8. Newman, J. C. and Raju, I. S., "Analyses of Surface Cracks in Finite Plates Under Tension or Bending Loads," NASA TP-1578, National Aeronautics and Space Administration, Washington, D.C., Dec. 1979.

9. Ditlevsen, O., Olsen, R., 1986. Statistical analysis of the virkler data on fatigue crack growth. Engineering Fracture Mechanics 25 (2), 177-195.

10. Lin YK, Yang JN. On statistical moments of fatigue crack propagation. Engng Fract Mech 1985; 18: 243–56.

11. Yang JN, Manning SD. Stochastic crack growth analysis methodologies for metallic structures. Engng Fract Mech 1990; 37: 1105–24.

12. Ishikawa, H., Tsurui, A., Tanaka, A.H., Ishikawa, H., 1993. Reliability assessment based upon probabilistic fracture mechanics.

13. Tsurui, A., Tanaka, A.H., 1987. Reliability degradation of structural components in the process of fatigue crack propagation under stationary random loading. Engng Fract Mech Vol. 27, No. 5, pp. 501-516, 1987

14. C. Rasmussen. *Evaluation of Gaussian processes and other methods for non-linear regression*. PhD thesis, University of Toronto, 1996.

15. J. Martin and T. Simpson. Use of kriging models to approximate deterministic computer models. AIAA Journal, 43(4):853–863, 2005.

16. Johnson, K, L., The strength of surfaces in rolling contact. Proceedings of the Institute of Mechanical Engineering, IMechE, pp. 203:151-63, 1989.

17. Ekberg, A., Kabo, E., Fatigue of railway wheels and rails under rolling contact and thermal loading – an overview. Wear, Vol. 258, Issue 7-8, pp. 1288-300, 2005.

18. Liu, Y., Mahadevan, S., Threshold intensity factor and crack growth rate prediction under mixed-mode loading. Engineering Fracture Mechanics, Vol. 74, pp. 332-345, 2007.

19. Virkler, D. A., Hillberry, B. M., Goel, P. K., The statistical nature of fatigue crack propagation. Technical Report Affdl-TR-78-43 Final Report - June 1976 to May 1978